# NANOPHASE PRECIPITATION STRENGTHENED AL ALLOYS PROCESSED THROUGH THE AMORPHOUS STATE

**Publication number:** WO03104505

**Publication date:** 2003-12-18

**Inventor:** OLSON GREGORY B (US); TANG WEIJIA (US); QIU CAIAN (US); JOU HERNG-JENG (US)

**Applicant:** QUESTEK INNOVATIONS LLC (US); OLSON GREGORY B (US); TANG WEIJIA (US); QIU CAIAN (US); JOU HERNG-JENG (US)

**Classification:**

**- International:** ***B22D23/00; C22C1/00; C22C21/00; C22C45/08; C22F1/00; C22F1/04;*** **B22D23/00; C22C1/00; C22C21/00; C22C45/00; C22F1/00; C22F1/04;** (IPC1-7): C22C

**- European:** C22C21/00; C22C45/08; C22F1/04

**Application number:** WO2003US12622 20030424

**Priority number(s):** US20020375940P 20020424; US20030450114P 20030225

**Also published as:**

- WO03104505 (A3)
- EP1499753 (A3)
- EP1499753 (A2)
- EP1499753 (A0)
- AU2003265234 (A1)

**Cited documents:**

- US5397403
- XP008025999
- XP001172942
- XP008025988
- XP008025998

**Report a data error here**

Abstract of **WO03104505**

Aluminum alloys having improved strength characteristics at elevated temperatures (300 DEG C) are manufactured by combining selected transition metals (Ni, Co, Ti, Fe, Y, Sc) and selected rare earth materials (Er, Tm, Yb, Lu) in amounts of about 2 to 12% and 2 to 15% atomic percent respectively in an amorphous, glassy state and subsequently devitrifying the amorphous material to form a crystalline mix of fcc and L12 phase material. Devitrification from the amorphous state may be effected by various means including thermal and thermo mechanical processes.

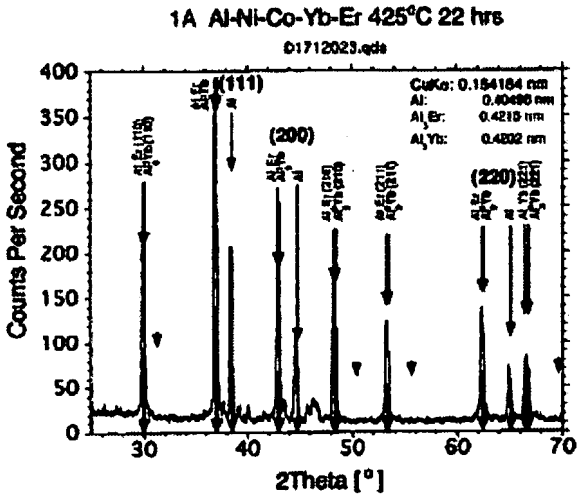

(12) INTERNATIONAL APPLICATION PUBLISHED UNDER THE PATENT COOPERATION TREATY (PCT)

(19) World Intellectual Property Organization
International Bureau

(43) International Publication Date
18 December 2003 (18.12.2003)

PCT

(10) International Publication Number
WO 03/104505 A2

(51) International Patent Classification[7]: C22C

(21) International Application Number: PCT/US03/12622

(22) International Filing Date: 24 April 2003 (24.04.2003)

(25) Filing Language: English

(26) Publication Language: English

(30) Priority Data:
60/375,940 24 April 2002 (24.04.2002) US
60/450,114 25 February 2003 (25.02.2003) US

(71) Applicant *(for all designated States except US)*: **QUESTEK INNOVATIONS LLC** [US/US]; 1820 Ridge Avenue, Evanston, IL 60201 (US).

(72) Inventors; and

(75) Inventors/Applicants *(for US only)*: **OLSON, Gregory, B.** [US/US]; 1363 Kenilwood, Riverwoods, IL 60015 (US). **TANG, Weijia** [CN/US]; 3144 Greenleaf Avenue, Wilmette, IL 60091 (US). **QIU, Caian** [CN/US]; 3144 Greenleaf Avenue, Wilmette, IL 60091 (US). **JOU, Herng-Jeng** [US/US]; 1210 Manor Drive, Wilmette, IL 60091 (US).

(74) Agent: **NELSON, Jon, O.**; Banner & Witcoff, Ltd., 10 South Wacker Drive, Suite 3000, Chicago, IL 60606-7402 (US).

(81) Designated States *(national)*: AE, AG, AL, AM, AT, AU, AZ, BA, BB, BG, BR, BY, BZ, CA, CH, CN, CO, CR, CU, CZ, DE, DK, DM, DZ, EC, EE, ES, FI, GB, GD, GE, GH, GM, HR, HU, ID, IL, IN, IS, JP, KE, KG, KP, KR, KZ, LC, LK, LR, LS, LT, LU, LV, MA, MD, MG, MK, MN, MW, MX, MZ, NI, NO, NZ, OM, PH, PL, PT, RO, RU, SC, SD, SE, SG, SK, SL, TJ, TM, TN, TR, TT, TZ, UA, UG, US, UZ, VC, VN, YU, ZA, ZM, ZW.

(84) Designated States *(regional)*: ARIPO patent (GH, GM, KE, LS, MW, MZ, SD, SL, SZ, TZ, UG, ZM, ZW), Eurasian patent (AM, AZ, BY, KG, KZ, MD, RU, TJ, TM), European patent (AT, BE, BG, CH, CY, CZ, DE, DK, EE, ES, FI, FR, GB, GR, HU, IE, IT, LU, MC, NL, PT, RO, SE, SI, SK, TR), OAPI patent (BF, BJ, CF, CG, CI, CM, GA, GN, GQ, GW, ML, MR, NE, SN, TD, TG).

**Published:**
— *without international search report and to be republished upon receipt of that report*

*[Continued on next page]*

(54) Title: NANOPHASE PRECIPITATION STRENGTHENED AL ALLOYS PROCESSED THROUGH THE AMORPHOUS STATE

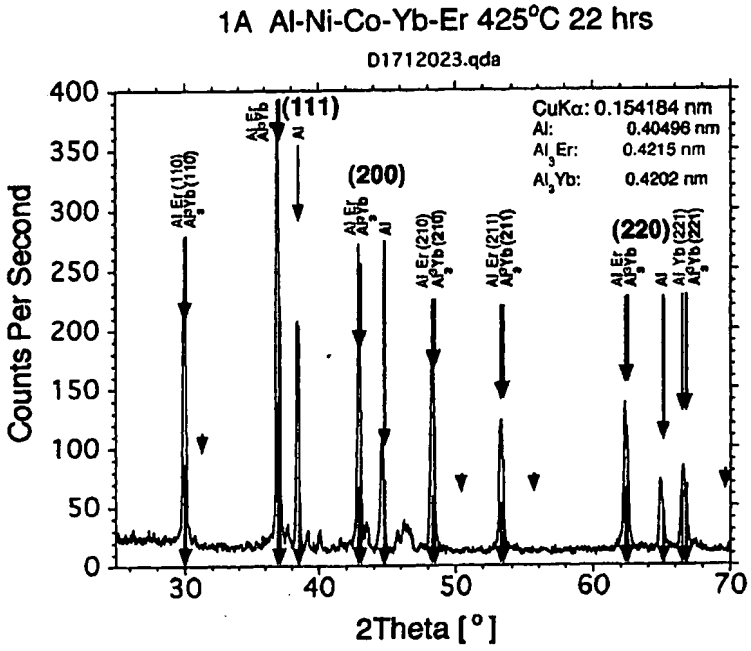


(57) Abstract: Aluminum alloys having improved strength characteristics at elevated temperatures (300°C) are manufactured by combining selected transition metals (Ni, Co, Ti, Fe, Y, Sc) and selected rare earth materials (Er, Tm, Yb, Lu) in amounts of about 2 to 12% and 2 to 15% atomic percent respectively in an amorphous, glassy state and subsequently devitrifying the amorphous material to form a crystalline mix of fcc and L12 phase material. Devitrification from the amorphous state may be effected by various means including thermal and thermo mechanical processes.

WO 03/104505 A2

*For two-letter codes and other abbreviations, refer to the "Guidance Notes on Codes and Abbreviations" appearing at the beginning of each regular issue of the PCT Gazette.*

# NANOPHASE PRECIPITATION STRENGTHENED Al ALLOYS PROCESSED THROUGH THE AMORPHOUS STATE

## BACKGROUND OF THE INVENTION

Activities relating to the development of the subject matter of this invention were funded at least in part by United States Government, U.S. Army Aviation & Missile Command Contract No. DAAH01-02-C-R125, and thus may be subject to license rights and other rights in the United States.

In a principal aspect, the present invention relates to aluminum-based alloys processed through an amorphous state or stage, preferably by means of a rapid solidification process from molten alloy, and then devitrified to a primarily crystalline structure by thermal or thermomechanical processing. In order to achieve a desired microstructure during processing, the aluminum alloy comprises a combination of rare earth and transition metal components with the aluminum. The final crystalline microstructure has stable high temperature strength (at or above about 300°C) characterized by nanoscale intermetallic precipitates, preferably $L1_2$ phase precipitates.

Currently available commercial aluminum alloys, either manufactured with ingot or powder processing, are not capable of simultaneously achieving high strength and high temperature stability near 300°C; such characteristics being particularly important in applications such as the fan components in turbine engines where short-term tensile strengths of the order of 500MPa (40-60 ksi) are desired. Precipitation hardening introduced by aging is a known method to strengthen aluminum alloys. Thus, conventional high strength aluminum alloys in commercial applications utilize GP (Guinier-Preston) zones and subsequent precipitation when seeking to achieve high material strength. With this type of strengthening, precipitates are usually formed during aging at or below 250°C in order to produce appropriate strengthening precipitate dispersions.

Examples of aluminum alloys processed with relatively high aging temperatures in commercial practice include 2618 (200°C for 20 hours), 4032 (170-175°C for 8-12 hours), and 2218 (240°C for 6 hours) [Metals Handbook — Properties and Selection: Nonferrous Alloys and Special-Purpose Materials, Volume 2, 10$^{th}$ Edition, ASM International]. At the noted aging temperatures, these alloys have improved microstructure stability relative to other commercial aluminum alloys. These aluminum alloys, when age-hardened, usually possess a room temperature yield strength of about 600Mpa (85 ksi). However, at temperatures approaching

300°C, the precipitation strengthening efficiency in these alloys quickly and significantly degrades as a result of precipitate coarsening and/or dissolution. Due to the unstable strengthening precipitate size distribution at such high temperatures, the yield strength of currently available aluminum alloys at 300°C is often only 10% of the yield strength at room temperature, and thus renders such alloys unsuitable for high temperature applications above 150°C.

In order to achieve a combination of high strength and usable high temperature properties in aluminum alloys, researchers have investigated a variety of intermetallic precipitation dispersions. Since selected intermetallic precipitates may determine the strength and ductility of the final aluminum alloy, it is desirable to select cubic precipitate phases with high crystallographic symmetry to promote ductility. The aluminum-based $L1_2$ phase (fcc ordered) is one of the best-known precipitates to achieve a good combination of high strength and high toughness.

However, since crystalline aluminum has very limited solubility for most intermetallics, including $L1_2$ forming components, it is difficult to produce fine intermetallic dispersions through crystalline solid-state heat treatments that utilize a step to dissolve the strengthening phase particles prior to reprecipitation during aging. However, rapid solidification processing (RSP) from the liquid state has been attempted or utilized. With an RSP process, it is possible to either (1) directly produce fine crystalline structure, or (2) produce partially or completely amorphous aluminum alloys. Nonetheless, crystalline RSP aluminum alloys have not been able to meet the high temperature strength requirements due to the difficulty of producing small, stable particle sizes at adequate volume fraction. Alternatively, the focus on amorphous aluminum alloys has been primarily on the glass formability. These glassy alloys in general have low ductility, and, when devitrified, they typically form crystalline microstructures that are far from optimal for fracture toughness and other requirements.

For example, RSP crystalline aluminum alloys, not designed to form glass with RSP, utilize a metastable and coherent $L1_2$ dispersion (about 1%) which converts into other phase structures at high temperature. [Parameswaran, Weertman and Fine, Scripta Metall., vol.23, pp.147, 1989] U.S. Pat. Nos. 4,950,452, 5,074,935, 5,334,266, 5,458,700, 5,431,751, 5,053,085 and its derived divisional patents (U.S. Pat. Nos. 5,240,517, 5,320,688, and 5,368,658) utilize RSP to achieve either amorphous, a mixture of amorphous and crystalline, or crystalline microstructures, without the use of an $L1_2$ strengthening dispersion. The aluminum alloys of U.S. Pat. No. 4,889,582 achieve the high temperature strength with RSP process and age

hardening to produce $Al_3Fe$ (which has non-cubic $DO_3$, not $L1_2$ structure) strengthening precipitates, using different alloying components. U.S. Pat. No. 4,464,199 describes high strength aluminum alloys with 4 to 15% iron processed with RSP to achieve high temperature stability. Use of iron promotes $Al_3Fe$ precipitation.

The aluminum alloys of U.S. Pat. No. 4,787,943 are composed of transition metals and rare earth metal components. However, with titanium and iron as the preferred transition metals, and gadolinium and cerium as rare earth elements, the alloy does not comprise a stable $L1_2$ strengthening dispersion.

U.S. Pat. No. 6,248,453B1 describes the use of an $L1_2$ strengthening dispersion for high strength aluminum alloys utilizing certain alloying components, but does not utilize a transition metal such as nickel and cobalt and an intermediate amorphous state as a means to refine the $L1_2$ microstructure.

Finally, the high strength and high temperature aluminum alloys referenced have not found widespread application due to the lack of robust processing to produce those alloys and the deficiency of other alloy properties, such as toughness and ductility.

## SUMMARY OF THE INVENTION

The present invention is directed to a new class of aluminum alloys characterized by formation from an intermediate amorphous state to a final face centered cubic (fcc) aluminum matrix strengthened by a precipitate dispersion in order to achieve high temperature strength with usable ductility. The disclosed aluminum alloys thus are comprised of a fine crystalline structure of primarily aluminum fcc matrix strengthened by a precipitate phase with high cubic symmetry, preferably the $L1_2$ phase. An appropriate melt of aluminum with crystalline formers is first processed to achieve an intermediate amorphous state to preserve the crystalline formers. The preferred method to achieve a primarily (above 70% in volume) amorphous state is a rapid solidification process (RSP) from the molten alloy by process techniques such as powder atomization, melt spinning, and spray casting. The RSP process preferably should have a cooling rate of at least about $10^3$°C/sec, preferably at least $10^4$°C/sec. Other methods to achieve amorphous microstructure through a solid-state process, such as mechanical milling, may also be used. The intermediate amorphous alloys are then devitrified to a final primarily (above 70% in volume) fcc/$L1_2$ crystalline microstructure with at least about 30% fcc phase in volume and at least about 10% $L1_2$ phase in volume. Thermal treatment, thermomechanical

treatment, or a combination of both, are the preferred methods to produce the final crystalline microstructure.

The alloys of the invention demonstrate high strength capability after both short and long exposure to a high temperature at or above 300°C by maintaining a fine and stable microstructure. For example, a short-term strength requirement of 40 – 60 ksi yield strength is expected. For the long-term strength, as characterized by creep strength, it has been demonstrated that optimal creep resistance at 300°C for aluminum alloys is obtained from a dispersion of 25 nm diameter $L1_2$ particles [E. A. Marquis, *Microstructural Evolution and Strengthening Mechanisms in Al-Sc and Al-Mg-Sc Alloys*, Ph.D. thesis, Northwestern University, 2002.]. Also, it has been demonstrated [Ohtera, Inoue and Masumoto, in *First International Conference on Processing Materials for Properties*, Ed. Henein and Oki, The Minerals, Metals & Materials Society, p.713, 1993] that aluminum-based alloys devitrified by extrusion from amorphous atomized powder can achieve aluminum fcc grain size of 80 to 170 nm, with intermetallic phase dispersions as fine as 10 to 80 nm in diameter. Such grain or particle sizes may therefore encompass the desired optimal particle diameter for creep strengthening by an $L1_2$ phase intermetallic dispersion. Accordingly, a process and an aluminum alloy product combining a sufficient amount of stable $L1_2$ refined or converted by devitrification from a glass phase material by appropriate thermal or thermomechanical processing has been discovered. The alloy meets or exceeds high temperature strength requirements with optimized creep resistance as a result of intermetallic, small particle phase dispersions.

The aluminum alloys of this invention are produced by combining aluminum, selected metals, particularly transition metals, rare earth elements, and other optional elements into a melt which is converted to an amorphous or glassy state and then subsequently to a crystalline state by a devitrification process. In the broadest sense about 2 to 15 atomic percent in the aggregate of at least one rare earth selected from the group consisting of erbium (Er), thulium (Tm), ytterbium (Yb) and lutetium (Lu) is provided for the melt. Further about 2 to 7 atomic percent in the aggregate of at least one transition metal selected from the group consisting of nickel (Ni), cobalt (Co), iron (Fe) and copper (Cu) is provided to enhance or facilitate the process step of forming an amorphous or glassy material from the melt. Other materials included, optionally, in the melt comprise additional transition metals, lithium (Li) and magnesium (Mg). For example, of less than about 5% in the aggregate by atomic fraction scandium (Sc), yttrium (Y), titanium (Ti), zirconium (Zr), vanadium (V), chromium (Cr),

manganese (Mn) and lithium (Li) incorporated into the melt or alloy as a modifier. Less than about 7% in the aggregate by atomic fraction magnesium (Mg), zinc (Zn), silver (Ag) and niobium (Nb) may be incorporated into the melt or alloy to accommodate fcc misfit in the crystalline state.

The selection of alloying components is based on the function or criteria of (1) good $L1_2$ formers, (2) adequate glass formability with RSP — this leads to the selection of components with strong short range ordering effects and slow long-range diffusing kinetics in molten aluminum, and (3) good fcc/$L1_2$ coherency with low misfit which lead to a fine microstructure and good coarsening resistance at high temperature.

Lanthanide rare earth $L1_2$ formers such as erbium (Er), thulium (Tm), ytterbium (Yb), and lutetium (Lu) are slow diffusers and hence enhance glass formability while at the same time allowing $L1_2$ formation during devitrification. Scandium (Sc) is a strong $L1_2$ former which can be used in conjunction with rare earth components to promote $L1_2$ formation and reduce the misfit between fcc and $L1_2$ phases. Transition metals such as nickel (Ni), cobalt (Co), iron (Fe), and copper (Cu) can enhance short range ordering in the molten aluminum, leading to the increase of glass transition temperature and promoting glass formability. Magnesium (Mg), as a component with relatively high solubility in crystalline aluminum, can be used in fcc aluminum to further reduce the fcc/$L1_2$ misfit.

With efficient precipitation strengthening by the $L1_2$ dispersion, the alloys of the subject invention achieve a hardness of 490 VHN at significantly higher aging temperature compared to conventional aluminum alloys indicating a usable strength at or beyond 300°C.

Thus, it is an object of the invention to provide a new class of high-strength $L1_2$ phase strengthened aluminum alloys processed into the amorphous state, preferably with a rapid solidification process, and then subsequently devitrified into a crystalline structure with a thermomechanical or thermal processes.

A further object of the invention is to provide aluminum alloys with usable strength at or above 300°C by selecting (1) slow diffusing $L1_2$ formers to prevent fast coarsening kinetics at high temperature, (2) appropriate matrix fcc and $L1_2$ components to reduce the lattice misfit between them to further slow down the coarsening kinetics and to promote the initial finer $L1_2$ morphology.

Another object of the invention is to utilize the cubic crystal structure of $L1_2$ phase to promote the interfacial coherency with an aluminum fcc matrix and the inherent ductile

behavior of the $L1_2$ crystalline phase itself, due to high number of slip systems in cubic $L1_2$ structure, to maintain reasonable overall alloy ductility.

A further object of the invention is to combine alloying components so that the $L1_2$ formation is enhanced while the likelihood of forming other undesirable intermetallics is reduced, in order to further promote alloy ductility of an aluminum alloy.

Another object of the invention is to provide adequate glass formability during the rapid solidification process such as powder atomization or melt spinning to form an amorphous aluminum alloy structure, preserving the $L1_2$ formers in the solution before a subsequent devitrification process.

A further object of the invention is to utilize the intermediate, highly supersaturated amorphous state, slow $L1_2$ coarsening kinetics, and low $L1_2$/fcc misfit to produce a fine microstructure in a strong aluminum alloy.

A further object of the invention is to provide aluminum alloys having high strength at high temperatures with appropriate toughness when processed with powder metallurgy techniques through an amorphous state.

Another object of the invention is to combine transition metals and rare earth components to provide sufficient glass formability during a rapid solidification process and a nanoscale $L1_2$ dispersion strengthened aluminum alloy fcc crystalline structure after devitrification.

These and other objects, advantages and features will be set forth in the detailed description which follows.

**BRIEF DESCRIPTION OF THE DRAWING**

In the detailed description which follows, reference will be made to the drawing comprised of the following figures:

**Figure 1** is a chart setting forth criteria for the design of aluminum alloys of the invention;

**Figure 2** is a diagram illustrating the viscosity of liquid aluminum nickel alloys calculated at 1700°C in comparison with experimental data wherein the comparison is based upon calculations made using different thermodynamic descriptions of the aluminum nickel liquid (substitutional solution model without associate or associate model with AlNi associate);

**Figure 3** is an assessed Al – Yb phase diagram in comparison with experimental data;

**Figure 4a** is a graph of the enthalpy of formation of cobalt and a rare earth, i.e. Er and Yb predicted by quantum mechanical calculation;

**Figure 4b** is a graph of the mixing enthalpy of the materials set forth in Figure 4a;

**Figure 4c** is a graph of the molar volume of the materials set forth in Figure 4a;

**Figure 5** is an X-ray diffractogram of the alloy of Example 1A as melt-spun with positions of fcc pure aluminum reflections indicating a fully amorphous state;

**Figure 6** is an isochronic DSC thermogram of the alloy of Example 1A indicating devitrification steps upon heating;

**Figure 7** is an X-ray diffractogram of the alloy of Example 1A after devitrification at 425°C for 22 hours, with positions of reflections of pure fcc Al, $Al_3Yb$, and $Al_3Er$ phases, indicating the desired phases: FCC+$L1_2$;

**Figure 8** is a SIMS elemental map of devitrified alloy of Example 1A indicating Er and Yb partition together to $L1_2$ phase, and NI and Co which do not partition to $L1_2$;

**Figure 9** is a scanning electron microscope (SEM) secondary electron image of devitrified alloy of Example 1A indicating submicron morphology;

**Figure 10** is a 3DAP microscopy reconstruction of $Al_3(Yb,Er)L1_2$ phase of the alloy of Example 1A after devitrification at 424°C for 19 hours;

**Figure 11** is an X-ray diffractogram of the alloy of Example 2A as melt-spun, with positions of fcc pure Al and $L1_2$ reflections, indicating fully amorphous status;

**Figure 12** is an X-ray diffractogram of the alloy of Example 2A after devitrification at 425°C for 19 hours, with positions of reflections of pure fcc Al, $Al_3Yb$, and $Al_3Er$ phases, indicating the desired phases: FCC+$L1_2$;

**Figure 13** is an X-ray diffractogram of the alloy of Example 2B as melt-spun, with positions of fcc pure Al and $L1_2$ reflections, indicating fully amorphous status;

**Figure 14** is an X-ray diffractogram of the alloy of Example 2B after devitrification at 425°C for 19 hours, with positions of reflections of pure fcc Al, $Al_3Yb$, and $Al_3Er$ phases, indicating the desired phases: FCC+$L1_2$ wherein the lattice parameter of $L1_2$ is reduced by Sc;

**Figure 15** is an X-ray diffractogram of the alloy of Example 2C as melt-spun, with positions of fcc pure Al and $L1_2$ reflections, indicating almost fully amorphous status;

**Figure 16** is an X-ray diffractogram of the alloy of Example 2C after devitrification at 425°C for 19 hours, with positions of reflections of pure fcc Al, $Al_3Yb$, and $Al_3Er$ phases, indicating the desired phases: FCC+$L1_2$ wherein the lattice parameter of $L1_2$ is expanded by Mg;

**Figure 17** is an X-ray diffractogram of the alloy of Example 2D as melt-spun, with positions of fcc pure Al and $L1_2$ reflections, indicating fully amorphous status;

**Figure 18** is an X-ray diffractogram of the alloy of Example 2D after devitrification at 425°C for 19 hours, with positions of reflections of pure fcc Al, $Al_3Yb$, and $Al_3Er$ phases, indicating the desired phases: FCC+$L1_2$ and wherein the lattice parameter of fcc is expanded by Mg and that of $L1_2$ is reduced by Sc;

**Figure 19** is an X-ray diffractogram of the alloy of Example 1C as melt-spun, with positions of fcc pure Al and $L1_2$ reflections, indicating non-amorphous status due to the absence of transition metal elements;

**Figure 20** is an X-ray diffractogram of the alloy of Example 1C after devitrification at 425°C for 19 hours, with positions of reflections of pure fcc Al, $Al_3Yb$, and $Al_3Er$ phases, indicating elements ER, Yb, and Sc can be completely intersoluble to form $L1_2$ and wherein the lattice parameter of $L1_2$ is reduced by Sc; and

**Figure 21** is a scanning electron microscope (SEM) secondary electron image of a devitrified alloy of Example 1C showing coarse microstructure in comparison with the alloy of Example 1A (see Figure 9) and indicating that passing through the glassy state can reduce the particle size of precipitation.

## DESCRIPTION OF THE PREFERRED EMBODIMENTS

General Summary

In general, the subject matter of the invention comprises a product (alloy) as well as a product by process and a process all directed to an aluminum alloy in crystalline form having higher or greater strength particularly at elevated temperatures, i.e. greater than at least 250°C and preferably 300°C. The alloy of aluminum is made by compounding a mixture of aluminum with selected rare earths (RE) and transition metals (TM) in an amorphous or glassy state followed by devitrification of the material from the amorphous state to a mixed crystalline state comprised of face centered cubic (fcc) and $L1_2$. (an ordered fcc) state wherein the ratios of the crystalline states is within certain preferred ranges. Preferably the resultant alloy has at least about 30% by volume fcc phase and at least about 10% by volume $L1_2$ phase material with limited residual amorphous or other phase material such as quasi-crystalline or ordered amorphous material.

The choice of starting materials may be varied as may the compounding processes, the glass phase formation processes and the devitrification processes. Importantly, when in the amorphous state, there may be some crystalline material contained therein, but preferably no more than about 30% by volume in the fcc phase. Thus forming the mixture in the amorphous or glassy intermediate state and subsequent devitrification constitute very important aspects of the invention.

The alloy materials, in addition to aluminum (Al), include one or more lanthanide rare earths (RE) selected or taken from the group of erbium (Er), thulium (Tm), ytterbium (Yb), and lutetium (Lu), and one or more transition metals (TM) taken or selected from the group of copper (Cu), nickel (Ni), cobalt (Co), titanium (Ti), iron (Fe), yttrium (Y), and scandium (Sc). Further additives in minor amounts (less than about five percent (5%) atomic percent) may be included such as magnesium (Mg). The range of various constituents is also important to maintain processability and preserve transition characteristics. Thus RE materials are utilized in the range of about 2 to 15 atomic percent (%), and the TM and metals are utilized in the aggregate range of about 2 to 12 atomic percent (%). Transition metals (TM) in the range of about 2 to 7 atomic percent are utilized.

The processes for mixing or forming the starting materials in the amorphous state are not necessarily limiting. Thus, it is contemplated that solid state processing, liquid or melt processing as well as gas phase processing may be utilized, though liquid phase processing is preferred based upon examples as reported hereinafter. The completeness of the amorphous state is preferably at least about 70% by volume and preferably greater. The amorphous state is a solid noncrystalline state or phase prior to devitrification.

Development Technique

Devitrification is accomplished via heat treating (thermal) processing, thermo-mechanical processing as well as other processing techniques.

Precipitation strengthened aluminum (Al) alloys are difficult to develop for high strength due to limited solubility of alloying elements in fcc Al. The low solubility of strengthening dispersion elements prevents the solid-state solution treatment of the alloy to bring strengthening components into solution. It is hence not necessarily possible to allow subsequent aging to produce a desirable strengthening microstructure. Al alloys with high fractions of precipitate that cannot be completely solution treated therefore have very coarse particle sizes that tend to limit strength, corrosion resistance and toughness. In contrast, the Al alloys exhibit composition

and microstructure characteristics that enable the Al alloys of invention to exhibit high strength, good ductility, and high temperature stability at or above 300°C.

By selecting an appropriate composition, processing techniques achieve a fully amorphous state after rapid cooling of the Al alloy composition. Furthermore, with careful selection of composition this glass can then be thermal or thermo-mechanically processed such that the glass devitrifies into a fully crystalline fcc matrix with intermetallic precipitates having a very fine size scale. By passing through the glass state, the equilibrium solidification that would produce coarse precipitates is avoided. Furthermore, the selection of the precipitate phase as $L1_2$ allows the precipitate to be coherent or semi-coherent with the fcc matrix improving the ductility of the alloy and the resistance of the precipitate to coarsen during subsequent thermal treatment.

Figure 1 is a system flow-block diagram that illustrates the processing/structure/properties relationships for alloys of the invention. The two-stage nature of the chart emphasizes the generally equal importance of processability and final performance in the design of alloys of the invention. The processability is governed by the glass forming ability; strength, ductility, and thermal stability are the required end properties.

Certain transition metals (TM) (such as Fe, Co, Ni, Cu) promote short-range ordering in liquid Al, which leads to low partial molar volume, low thermal expansion, and high viscosity that are beneficial to glass forming ability. Rare-earth (RE) elements (such as Ce, Gd, Yb, Er) with large atomic size exhibit low diffusivity in Al and thus retard crystal nucleation. Therefore, Al-TM-RE comprise a class of glass forming system for Al alloys.

Viscosity of liquid metals also has a strong effect on the glass forming ability. Liquid phase metals having high viscosity usually becomes glass through fast cooling. A binary model to describe liquid's viscosity is set forth in Equation (1):

$$\eta = -\frac{x_1 x_2}{RT}(x_1\eta_1^o + x_2\eta_2^o)\frac{\partial^2 G_m}{\partial x_2^2} \qquad (1)$$

The variables $x_i$ and $G_m$ represent the mole fraction and molar Gibbs energy of the liquid, respectively. The viscosity of pure components, $\eta_i^o$, is available from literature, see Table 1. From the above equation it is seen that the composition dependence of the viscosity is fully determined by the thermodynamic properties of the liquid.

Table 1. Viscosity and related data for pure liquid metals
**[L. Battezzati and A.L. Greer, "The Viscosity of Liquid Metals and Alloys," *Acta metall.* 37, 1791 (1989).]**

| Element | $T_m$ (K) | $V_m$ ($10^{-6}$ $m^3$/mol) | $\eta(T_m)$ ($10^{-3}$ Pa s) | $C_A$ [$10^{-7}$ $(J/K\ mol^{1/3})^{1/2}$] | E (kJ/mol) | B ($E/RT_m$) | $\eta_o$ ($10^{-3}$ Pa s) |
|---|---|---|---|---|---|---|---|
| Al | 933 | 11.3 | 1.30 | 1.30 | 16.5 | 2.13 | 0.149 |
| Co | 1765 | 7.59 | 4.18 | 1.58 | 44.4 | 3.03 | 0.255 |
| Cr | 2133 | 8.28 | 5.7 | ~2.2 | ~185 | ~10.43 | $1.7x10^{-4}$ |
| Cu | 1356 | 7.94 | 4.0 | 1.72 | 30.5 | 2.71 | 0.301 |
| Fe | 1809 | 7.96 | 5.5 | 2.18 | 41.4 | 2.75 | 0.370 |
| Mn | 1517 | 9.58 | 5 | 2.5 | 20-46.5 | 1.6-3.7 | 0.12-1.02 |
| Ni | 1728 | 7.43 | 4.90 | 1.85 | 50.2 | 3.49 | 0.166 |
| V | 2175 | 8.9 | 2.4 | 0.98 | ~73 | ~4.04 | ~0.042 |
| Ti | 1958 | 11.6 | 2.2 | 1.18 | ~68 | ~4.18 | ~0.034 |
| Zr | 2125 | ~15.7 | 3.5 | 1.58 | ~88 | ~4.98 | ~0.024 |

$T_m$: melting temperature $V_m$: molar volume at $T_m$ $\eta(T_m)$: viscosity at $T_m$
$C_A$: constant E: activation energy for viscous flow B: $B= E/RT_m$
$\eta_o$: pre-exponential viscosity

Equation (1) has been validated for several binary systems where both experimental viscosity data and thermodynamic descriptions are available. An example is the Al-Ni system where an intermediate compound AlNi melts congruently at about 1650°C. Figure 2 shows the calculated viscosity in Al-Ni liquid at 1700°C as a function of Ni content, in comparison with experimental data. It is seen that the calculated viscosity shows a similar trend as the experimental data, but the latter indicates a stronger increase of the viscosity around 50 at.% Ni. The strong increase in viscosity is believed to be caused by molecular associates of Al-Ni in the liquid. In order to illustrate the effect of the AlNi associates on the viscosity, the Al-Ni system was thermodynamically reassessed with an associate model for the liquid free energy. The viscosity of Al-Ni liquid calculated using the AlNi associate model is also plotted in Figure 2 for comparison. The calculation shows a significant increase in the viscosity due to the formation of liquid AlNi associates.

This viscosity model has further been extended to multi-component systems, which provides guidance of glass forming ability for the design of alloys of the invention.

A model to predict glass transition temperature, $T_g$, has been developed for the Al-TM-RE system. The model is based on the parabolic relationship between $T_g$ and room temperature glass shear modulus, G, and it assumes that G is linear in atomic fraction, X, of each element according to equation (2):

$$T_g = \left(14100 \sum_i K_i X_i\right)^{0.49} \qquad (2)$$

$$i = Al, Mg, Ni, Co, Er, Yb, Sc, Y, etc.$$

The coefficient for each element, $K_i$, has been calibrated to experimental DSC data of melt-spun amorphous ribbons. These coefficients quantitatively represent the relative effectiveness of the aforementioned molecular associates in promoting glass forming ability by varying $T_g$. This model also provides guidance of glass forming ability for the design of alloys of the invention. The prediction error of equation (2) compared to available experimental data is about 9 K with a standard deviation of 10 K, which is within the experimental precision.

The desired performance for applications (e.g. aircraft structural components, high temperature turbine components, etc.) determines a set of alloy properties required, including strength, ductility and thermal stability resistance up to 300°C. The desired properties can be achieved through a fine, stable, multicomponent $L1_2$ phase dispersion in the Al matrix after devitrification of the glassy Al, as long as a sufficient volume fraction of $L1_2$ and low misfit with the Al matrix and thus low coarsening rate can be obtained.

The elements Er, Lu, Tm and Yb are known as the only stable rare earth (RE) $L1_2$ formers. The melting point and cost of these rare earth elements are presented in Table 2. Some properties of corresponding trialuminides are also given in Table 2, including lattice parameter, density, and $L1_2$ decomposition or congruent melting temperature. Among the four RE elements, according to Table 2, Yb has the smallest lattice parameter and relatively lower cost. Er has the lowest cost. Both Yb and Er have relatively lower melting point. Usually, the lower the melting temperature, the higher the glass forming ability. As a consequence, Alloys of the invention utilize Yb and Er as preferred $L1_2$ formers rather than Tm and Lu.

Table 2. Stable $L1_2$ formers and their properties.

| Element | Melting Point | Cost[a] | $L1_2$ | Lattice Parameter | Density | $L1_2$ Max. Temp. |
|---|---|---|---|---|---|---|
| Er | 1529°C | $725/kg | $Al_3Er$ | 4.226 Å | 5.507 g/cm$^3$ | 1070°C |
| Lu | 1663°C | $7500/kg | $Al_3Lu$ | 4.186 Å | 5.783 g/cm$^3$ | 1200°C |
| Tm | 1545°C | $6500/kg | $Al_3Tm$ | 4.203 Å | 5.591 g/cm$^3$ | |
| Yb | 819°C | $1600/kg | $Al_3Yb$ | 4.202 Å | 5.682 g/cm$^3$ | 980°C |
| Sc | 1541°C | $18,000/kg | $Al_3Sc$ | 4.101 Å | 3.03 g/cm$^3$ | 1320°C |

[a] For 1-5 kg cast metal ingots from 99.9%-grade oxides

Sc is the only transition metal (TM) element that can form a stable $L1_2$ with Al. In comparison with RE $L1_2$ formers, Sc can form $L1_2$ with a smaller lattice parameter of 4.101 Å,

thus leading to smaller misfit between $L1_2$ and the Al matrix. However, Sc is by far the most expensive of the elements considered, as seen in Table 2. The alloy of the invention therefore seeks to limit the use of Sc as much as possible. Efforts have been made to search for other transition metals to substitute for Sc. A preliminary requirement for such substitution is solubility. Experiments have shown that Ti has a substantial solubility in $Al_3Sc$, up to 12.5 at.%, i.e. $Al_{0.75}Sc_{0.125}Ti_{0.125}$. In addition, Ti has the lowest diffusion coefficient in solid Al among the transition metals. For instance, the diffusivity in Al at 300°C is $9.0\times10^{-20}$ $m^2/s$ for Sc, $6.3\times10^{-24}$ $m^2/s$ for Zr, and $2.7\times10^{-25}$ $m^2/s$ for Ti. Adding Ti to $Al_3Sc$ will thus reduce the coarsening rate of $L1_2$ precipitates. Moreover, addition of Ti decreases the lattice parameter of $Al_3(Sc,Ti)$ and hence minimizes the lattice misfit with Al. The lattice parameters for seven hypothetical $L1_2$ compounds with transition metals are calculated at zero degree Kelvin (0 K) using the first-principle quantum mechanical approach. Results are shown in Table 3. All seven hypothetic $L1_2$ compounds show significant smaller lattice parameters than those stable $L1_2$ phases. Thus, alloys of the invention incorporate Yb, Er and Sc as base $L1_2$ formers but are not limited to these elements. TMs such as Ti, V, Zr, etc, which will result in low misfit and thus lower interfacial energy to yield a low driving force for particle coarsening are considered useful.

Table 3 Lattice Parameters of hypothetical $L1_2$ TM Compounds through First Principle Calculations at 0 K.

| TMs Hypothetic $L1_2$ | Lattice Parameter, Å |
|---|---|
| $Al_3Ti$ | 3.967 |
| $Al_3Zr$ | 4.085 |
| $Al_3V$ | 4.045 |
| $Al_3Fe$ | 3.8005 |
| $Al_3Ni$ | 3.8469 |
| $Al_3Co$ | 3.7946 |
| $Al_3Cu$ | 3.9363 |

It should be pointed out that the compound $Al_3Ti$ is metastable as the $L1_2$ phase but stable as $D0_{22}$. It can be transformed to the $L1_2$ structure if Al is substituted partially by Cr, Mn, Fe, Co or Ni.

For a multicomponent $L1_2$ phase, the lattice parameter $a$ can be calculated based on a linear model similar to Vegard's law. As an example, we have the following equation for $L1_2$ with the formula $Al_3(Er_xYb_ySc_z)$ is utilized:

$$a[Al_3(Er_xYb_ySc_z] = x * a(Al_3Er) + y * a(Al_3Yb) + z * a(Al_3Sc) \quad (3)$$

Assuming $L1_2$ has a linear thermal expansion, its lattice parameter at elevated temperature can be calculated as follows (T in °C):

$$a(L1_2, T) = a(L1_2, RT) \times [1 + (T - 25) \times \alpha(L1_2)] \quad (4)$$

where $\alpha(L1_2)$ represents the thermal expansion estimated according to the following reciprocal relation:

$$\frac{\alpha(M)}{\alpha(Al_3M)} = \frac{T_m(Al_3M)}{T_m(M)} \quad (5)$$

where M represents the corresponding pure metal in $Al_3M$ and $T_m$ is the melting point (°K). Table 4 summarizes melting point, thermal expansion of relevant elements in alloys of the invention and the estimated thermal expansion as well as lattice parameter at 25°C and 300°C for stable $L1_2$ or meta-stable $L1_2$.

Table 4. Estimation of Thermal Expansion Coefficients and Lattice Parameters.

| Element | Melting Point, °K | Thermal Expansion, 1/°K, 20~100°C | Thermal Expansion, 1/°K, 20~300°C | $L1_2$ Alloys | Melting Point, °K | Thermal Expansion, 20~300°C | Lattice Parameter, Å, 25°C | Lattice Parameter, Å, 300°C |
|---|---|---|---|---|---|---|---|---|
| Ni | 1728 | $13.3\times10^{-6}$ | $14.4\times10^{-6}$ | $Al_3Ni$ | 913 | $27.254\times10^{-6}$ | 3.8639 | 3.8929 |
| Co | 1768 | $12.5\times10^{-6}$ | $13.6\times10^{-6}$ | $Al_3Co$ | 1408 | $17.077\times10^{-6}$ | 3.8114 | 3.8293 |
| Yb | 1092 | $25\times10^{-6}$ | $25\times10^{-6}$ | $Al_3Yb$ | 1253 | $21.788\times10^{-6}$ | 4.202 | 4.2272 |
| Er | 1802 | $9.2\times10^{-6}$ | $9.2\times10^{-6}$ | $Al_3Er$ | 1343 | $12.344\times10^{-6}$ | 4.226 | 4.2403 |
| Sc | 1814 | $12\times10^{-6}$ | $12\times10^{-6}$ | $Al_3Sc$ | 1593 | 13.665 | 4.101 | 4.1164 |
| Ti | 1943 | $8.9\times10^{-6}$ | $9.2\times10^{-6}$ | $Al_3Ti$ | 1623 | 11.014 | 3.967 | 3.979 |
| Y | 1795 | $10.8\times10^{-6}$ | $10.8\times10^{-6}$ | $Al_3Y$ | 1253 | 15.472 | 4.299 | 4.3173 |
| Al | | | $25.3\times10^{-6}$ | | | | 4.0497 | 4.0779 |

In the practice of the invention, decrease of the misfit by expanding the lattice parameter of the Al matrix is a useful technique. There are few elements that have significant solubility in Al. Mg is the only one that can substantially increase the lattice spacing of Al. According to literature information, in dilute AlMg alloys, every one atom percent of Mg will expand the Al lattice by 0.0045 Å. Further, every one atom percent of Mg will increase the linear coefficient of thermal expansion of Al by $1.179\times10^{-7}$/°C.

Thermodynamic modeling and assessments have been performed for Al-TM-RE systems with relevant elements incorporated in alloys of the invention. The assessed Al-Yb binary phase diagram is shown in Figure 3. The $L1_2$ $Al_3Yb$ is the strengthening phase that is used in alloys of the invention. According to Figure 3, $Al_3Yb$ is not solution treatable. The only way to avoid coarse precipitation from Al liquid is using fast cooling. It is possible to get fine

crystalline precipitates directly by rapid solidification processing (RSP) from the melt. However, much finer precipitates can be generated through devitrification of amorphous state due to the larger driving force. In addition, the precipitation process can be controlled through devitrification.

Quantum mechanical calculations have been performed in $Al_3Er$-$Al_3Co$ and $Al_3Yb$-$Al_3Co$ systems. The predicted enthalpy of formation, mixing enthalpy and molar volume in the corresponding systems are plotted in Figure 4. According to Figure 4, there is a strong repulsive Co-RE interaction indicating negligible Co solubility in $L1_2$ $Al_3RE$. This sets a challenge in producing good glass forming alloys through conventional technology in the same composition intended to precipitate a significant amount of $L1_2$ precipitation through devitrification.

Experimental Results

The present invention alloys, through computational design of multi-component Al-TM-RE systems incorporate, desired processing properties – glass forming ability and the desired microstructure – a fine dispersion of $L1_2$ after devitrification in the Al matrix. Alloys of the invention are summarized in Table 5 for their composition, status in melt-spun and devitrification conditions, as well as the lattice parameter of the Al fcc and the $L1_2$ phases and the misfit between $L1_2$ and Al matrix.

Table 5 Summary of Composition and Microstructure of Al Alloys

| No. | Alloy Composition at.% | As-spun status | Main phases after devitrfication | Lattice Parameter | | Misfit % |
|---|---|---|---|---|---|---|
| | | | | $L1_2$, a(Å) | fcc, a(Å) | |
| 1A | Al-2.5Ni-2.5Co -3.5Yb-3.5Er | fully glass | fcc, $L1_2$ + minor x phase | 4.215 | 4.063 | 3.735 |
| 1B | Al-2.75Ni-2.75Co-2.17Yb -2.17Er-2.17Y | fully glass | fcc, $L1_2$+$Al_3Y$+ minor x phase | 4.217 | 4.050 | 4.123 |
| 1C | Al-6Yb-6Er | fcc, $L1_2$ + some glass | fcc, $L1_2$ | 4.208 | 4.057 | 3.726 |
| 1D | Al-4Yb-4Er-4Y | fcc, $L1_2$ + some glass | fcc, $L1_2$ + $Al_3Y$ | 4.229 | 4.059 | 4.192 |
| 1E | Al-4.5Yb-4.5Er-3Sc | fcc, $L1_2$ + some glass | fcc, $L1_2$ | 4.183 | 4.060 | 3.032 |
| 1F | Al-12Er-3Mg | fcc, $L1_2$ + some glass | fcc, $L1_2$ | 4.216 | 4.059 | 3.865 |
| 1G | Al-12Er-6Mg | fcc, $L1_2$ + some glass | fcc, $L1_2$ | 4.217 | 4.065 | 3.739 |
| 1H | Al-12Yb-3Mg | fcc + some glass | fcc, $L1_2$ | 4.216 | 4.076 | 3.435 |
| 1I | Al-12Yb-6Mg | fcc, $L1_2$ + some glass | fcc, $L1_2$ | 4.191 | 4.061 | 3.201 |
| 2A | Al-2Ni-2Co-4Yb-4Er | almost fully glass+minor fcc | fcc, $L1_2$ + minor x phase | 4.201 | 4.049 | 3.754 |
| 2B | Al-2.5Ni-2.5Co-2Yb-2Er-3Sc | almost fully glass+minor fcc | fcc, $L1_2$ + minor x phase | 4.150 | 4.048 | 2.520 |
| 2C | Al-3Mg-2.5Ni-2.5Co-4.5Yb-2.5Er | mostly glass + minor fcc | fcc, $L1_2$ + minor x phase | 4.197 | 4.060 | 3.374 |
| 2D | Al-3Mg-2.5Ni-2.5Co-2.5Yb-1.5Er-3Sc | fully glass | fcc, $L1_2$ + minor x phase | 4.155 | 4.057 | 2.416 |

According to Table 5, alloys with TM elements (e.g. Ni and Co) are fully glass or almost fully glass in the as melt-spun conditions. These alloys include alloy 1A, 1B, 2A, 2B, 2C and 2D. Alloys without Ni and Co primarily show FCC Al and $L1_2$ crystalline phases although they are partially amorphous in the as melt-spun conditions. These alloys include alloy 1C, 1D, 1E, 1F, 1G, 1H and 1I. The results confirm the prediction that TM elements such as Ni and Co are critical elements to promote the glass forming ability in the alloys of the invention. Through devitrification, all alloys precipitate mainly $L1_2$ in the Al matrix. It should be emphasized that the particle size of alloys passing through a fully or almost fully glassy state is much finer than that of alloys without passing through the glassy state or only passing through a partially glassy state with $L1_2$ already present in the as-spun condition.

Following is a detailed demonstration of characteristics of alloys in Table 5.

**Example 1**

Alloy 1A in Table 5 was fabricated into both powders using gas atomization and ribbons using melt spinning technology (wheel speed 55 m/s). In the as melt-spun condition, Alloy 1A was initially characterized by X-ray diffraction (XRD) and differential scanning calorimetry (DSC). The diffractometer trace (Cu-Kα radiation ) of as-spun Alloy 1A in Figure 5 shows a broad peak characteristic of glass, and the ribbons show very good ductility, also characteristic of the glassy state. A DSC trace run at 40°C/min. shown in Figure 6 indicates three stages of glass devitrification at temperatures near 200°C, 315°C and 370°C.

DSC thermograms indicated that for heating at a constant rate of 10-40°C/min, the dominant crystallization reactions occur below about 400°C for all alloys under investigation. Based on this information, a temperature of 425°C was selected for the devitrification anneal. Specifically, alloy samples were encapsulated in quartz tubes under a protective atmosphere of approximately 500 mbar Argon with 99.999% purity. The encapsulated specimens were kept at 425°C for periods of 19 or 22 hrs, respectively, to ensure completion of the crystallization reaction and grain growth to a size that facilitates experimental characterization.

Figure 7 shows an X-ray diffractogram of Alloy 1A after devitrification at 425°C for 22 hours. At this point transformations I-III are fully completed and the ribbons are fully devitrified in the sense that no significant amount of amorphous material can be detected by XRD and TEM. The peak positions of (111), (200), and (220) reflections calculated for FCC pure Al (lattice parameter 4.0496 Å) are indicated in red. Within the accuracy of this experiment (that is 0.01° at $2\theta = 38.505°$ (Al (111)), the measured peak positions are identical to pure Al, indicating the equilibrium solubility of Ni, Co, Yb, and Er in Al is very small. Also marked in red are the positions of the 'forbidden' reflections (110), (210), (211), and (221) for FCC Al, which are superlattice reflections of the $L1_2$ structure. The peak positions for $L1_2$ $Al_3Yb$ (lattice parameter 4.202 Å marked in green, and that for $L1_2$ $Al_3Er$ (lattice parameter 4.215 Å) are marked in brown. It can be seen that the measured peak positions are perfectly matched by $L1_2$ structure reflections. Therefore, Alloy 1A mainly consists of FCC Al and $L1_2$ phases as devitrified microstructure. It is also noticed that there is a minor third phase *x*, which crystalline structure is to be identified.

The FCC Al+$L1_2$ microstructure of Alloy 1A was investigated by the secondary ion mass spectrometry (SIMS) technology. Figure 8 indicates that Yb and Er partition together into $L1_2$ precipitates, while Ni and Co have limited partitions.

The morphology of FCC+$L1_2$ microstructure of Alloy 1A is shown in Figure 9. This SEM secondary electron image indicates that the majority of $L1_2$ precipitates are less than 1 micron after devitrification at 425°C, 22 hours. Based upon previously discussed experience in devitrified Al alloys, this indicated the potential to obtain nanoscale $L1_2$ precipitates with thermomechanical processing.

The three dimension atom probe microscopy (3DAPM) analysis confirms that $L1_2$ exists in Alloy 1A with formula $Al_{0.72}(Yb,Er)_{0.28}$. Yb and Er have about the same site fraction. Ni and Co are negligible in $L1_2$ phase. See Figure 10.

Alloy 1A was also studied through microhardness testing in ribbon conditions after thermal cycles required for powder consolidation and extrusion. Results are presented in Table 6. Through devitrification at a temperature near 300°C, Alloy 1A has demonstrated a hardness of 490 VHN, which is equivalent to the room temperature tensile strength exceeding 1000 MPa according to Inoue's work in similar alloy systems. (Akihisa Inoue, "Amorphous, nanoquasicrystalline and nanocrystalline alloys in Al-based systems", Progress in Materials Science 43 (1998) 365-520). This result indicates high efficient strengthening of $L1_2$.

Table 6 Microhardness testing of Alloy 1A

| Condition | Hardness (VHN) |
|---|---|
| As-spun | 369 |
| 177°C 1hr | 276 |
| 177°C 10hrs | 310 |
| 177°C 20 hrs | 335 |
| 177°C 20hrs then 288°C 2hrs. | 490 |
| 177°C 20hrs then 316°C 2hrs. | 340 |
| 177°C 20hrs then 400°C 2hrs. | 275 |

**Example 2**

Alloy 2A in Table 5 was fabricated into ribbons using melt spinning technology (wheel speed 55 m/s). In the as melt-spun condition, Alloy 2A was characterized by X-ray diffraction. The diffractometer trace (Cu-Kα radiation ) of as-spun Alloy 2A in Figure 11 shows a broad

peak characteristic of glass, and the ribbons show reasonable good ductility, also characteristic of the glassy state.

Figure 12 shows an X-ray diffractogram of Alloy 2A after devitrification at 425°C for 19 hours. At this point the ribbon is fully devitrified in the sense that no significant amount of amorphous material can be detected by XRD. The peak positions of (111), (200), and (220) reflections calculated for FCC pure Al (lattice parameter 0.40496 Å) are indicated in red. The measured peak positions are identical to pure Al, indicating the equilibrium solubility of Ni, Co, Yb, and Er in Al is very small. Also marked in red are the positions of the 'forbidden' reflections (110), (210), (211), and (221) for FCC Al, which are superlattice reflections of the $L1_2$ structure. The peak positions for $L1_2$ $Al_3Yb$ (lattice parameter 4.202 Å) are marked in green, and that for $L1_2$ $Al_3Er$ (lattice parameter 4.215 Å) are marked in brown. It can be seen that the measured peak positions are perfectly matched by $L1_2$ structure reflections. Therefore, Alloy 2A mainly consists of FCC Al and $L1_2$ phases as devitrified microstructure. It is noticed that the third phase *x*, in Example 2A, is less than in Example 1A, reflecting the desire to reduce the amount of *x* phase by reducing Ni and Co in Alloy 2A while retaining reasonable glass forming ability.

**Example 3**

Alloy 2B in Table 5 was fabricated into ribbons using melt spinning technology (wheel speed 55 m/s). In the as melt-spun condition, Alloy 2B was characterized by X-ray diffraction. The diffractometer trace (Cu-Kα radiation) of as-spun Alloy 2B in Figure 13 shows a broad peak characteristic of glass, and the ribbons show reasonable good ductility, also characteristic of the glassy state.

Figure 14 shows an X-ray diffractogram of Alloy 2B after devitrification at 425°C for 19 hours. At this point the ribbon is fully devitrified in the sense that no significant amount of amorphous material can be detected by X-ray diffraction (XRD). The peak positions of (111), (200), and (220) reflections calculated for FCC pure Al (lattice parameter 4.0496 Å) are indicated in red. The measured peak positions are identical to pure Al, indicating the equilibrium solubility of Ni, Co, Yb, Er and Sc in Al is very small. Also marked in red are the positions of the 'forbidden' reflections (110), (210), (211), and (221) for FCC Al, which are superlattice reflections of the $L1_2$ structure. It can be seen that the measured peak positions are matched by $L1_2$ structure reflections with lattice parameter 4.150 Å. It demonstrates that Yb, Er and Sc can be completely intersoluble to form $L1_2$, and the lattice parameter has been

significantly reduced by adding Sc, which is another means of reducing misfit to keep the $L1_2$ precipitates coarsening resistant. The misfit between FCC Al and $L1_2$ is 2.52% for Alloy 2B.

**Example 4**

Alloy 2C in Table 5 was fabricated into ribbons using melt spinning technology (wheel speed 55 m/s). In the as melt-spun condition, Alloy 2C was characterized by X-ray diffraction. The diffractometer trace (Cu-Kα radiation ) of as-spun Alloy 2C in Figure 15 shows a broad peak characteristic of glass, and the ribbons show reasonable good ductility, also characteristic of the glassy state.

Figure 16 shows an X-ray diffractogram of Alloy 2C after devitrification at 425°C for 19 hours. At this point the ribbon is fully devitrified in the sense that no significant amount of amorphous material can be detected by XRD. The peak positions of (111), (200), and (220) reflections calculated for FCC pure Al (lattice parameter 4.0496 Å) are indicated in red. The measured peak positions indicate that the lattice space of Al has been dilated to 4.060 Å, reflecting another feature of the invention: adding Mg to expand the lattice space of Al and thus decrease the misfit between Al and $L1_2$. Also marked in red are the positions of the 'forbidden' reflections (110), (210), (211), and (221) for FCC Al, which are superlattice reflections of the $L1_2$ structure. It can be seen that the measured peak positions are perfectly matched by $L1_2$ structure reflections. Therefore, Alloy 2C mainly consists of FCC Al and $L1_2$ phases as devitrified microstructure.

**Example 5**

Alloy 2D in Table 5 was fabricated into ribbons using melt spinning technology (wheel speed 55 m/s). In the as melt-spun condition, Alloy 2D was characterized by X-ray diffraction. The diffractometer trace (Cu-Kα radiation ) of as-spun Alloy 2D in Figure 17 shows a broad peak characteristic of glass, and the ribbons show very good ductility, also characteristic of the glassy state.

Figure 18 shows an X-ray diffractogram of Alloy 2D after devitrification at 425°C for 19 hours. At this point the ribbon is fully devitrified in the sense that no significant amount of amorphous material can be detected by XRD. The peak positions of (111), (200), and (220) reflections calculated for FCC pure Al (lattice parameter 4.0496 Å) are indicated in red. The measured peak positions indicate that the lattice space of Al has been dilated to 4.057 Å. Also marked in red are the positions of the 'forbidden' reflections (110), (210), (211), and (221) for

FCC Al, which are superlattice reflections of the $L1_2$ structure. It can be seen that the measured peak positions are matched by $L1_2$ structure reflections with lattice parameter 4.155 Å. It demonstrates that Yb, Er and Sc can be completely intersoluble to form $L1_2$, and the lattice parameter has been significantly reduced by adding Sc. Alloy 2D reflects the means of reducing misfit by adding Mg to dilate the lattice space of Al and adding Sc to decrease the lattice parameter of $L1_2$. Thus Alloy 2D achieved the lowest misfit so far:2.42% without losing the glass forming ability. Alloy 2D mainly consists of FCC Al and $L1_2$ phases as devitrified microstructure.

**Example 6**

Alloy 1E in Table 5 was fabricated into ribbons using melt spinning technology (wheel speed 55 m/s). In the as melt-spun condition, Alloy 1E was characterized by X-ray diffraction. The diffractometer trace (Cu-Kα radiation ) of as-spun Alloy 1E in Figure 19 shows crystalline reflection peaks, indicating non-amorphous or partially non-amorphous state. It demonstrates that TMs are necessary elements to promote glass in Al-TM-RE system. In addition, the ribbons are very brittle, also characteristic of the non-glassy state.

Figure 20 shows an X-ray diffractogram of Alloy 1E after devitrification at 425°C for 19 hours. This diffractogram shows that Alloy 1E only has two phases: fcc Al+$L1_2$. It also demonstrates that Yb, Er and Sc can be completely intersoluble to form $L1_2$, and the lattice parameter has been significantly reduced by adding Sc. The misfit between FCC Al and $L1_2$ is 3.03%.

The morphology of fcc+$L1_2$ microstructure of Alloy 1E is shown in Figure 21. This SEM secondary electron image indicates that the particle size of $L1_2$ precipitates is about 3 times larger than that of Alloy 1A, see Figure 9, although the misfit of Alloy 1A is a little bit larger:3.735%. It indicates that devitrification of glassy state can significantly reduce the particle size of precipitation in comparison with that by crystallization directly from fast cooling at the same rate.

In review, the range of composition processing parameters, microstructure characterization and physical properties is summarized in the following Table 7:

Table 7

| | Composition | | | | | Processing Parameters | | | microstructure characterization (vol %) | | | | | | | Properties | |
|---|---|---|---|---|---|---|---|---|---|---|---|---|---|---|---|---|---|
| | Rare Earth Elem. | Transition Metals and Mg, Li | | | | glass | thermal | thermo-mechan-ical | amorphous | | | devitrified state | | | | | |
| | (1) | Late TM for glass forming (2) | L12 modi-fier (3) | FCC elem. For misfit (4) | at.% | RSP | aging temp. for thermal devitrifying | hot extrusion parameters | fcc | glass | others | fcc | L12 | glass | others | room tempera-ture UTS | high tempera-ture UTS of 275-410 Mpa |
| Maximum Ranges | Er,Lu, Yb,Tm U | Ni,Co, Fe,Cu | Sc,Y Ti,Zr, V,Cr, Mn,U, Nb | Mg,Zn, Ag | 2%<sum(group (1))<16% 2%<sum(group (2))<7% sum(group (3))<5% sum(group (4))<7% | cooling rate >$10^4$°C /sec | >300°C | | <15% | bal. | <10% | bal. | >10% | <15% | <20% | >500MPa | >250°C |
| Preferred Ranges | Er,Lu, Yb,Tm | Ni,Co | Sc | Mg | 5%<sum(group (1))<12% 2%<sum(group (2))<7% Sc<4% Mg<6% | cooling rate >$10^4$°C /sec | >325°C <475°C | >350°C <450°C 5,9,11:1 ratio | <8% | bal. | <3% | bal. | >20-25% | <8% | <15% | >800MPa | >275°C |
| Optimum Ranges | Er,Yb, | Ni,Co | Sc | | 7%<sum(Er,Yb,Sc)<8% 3%<sum(Ni,Co)<6% | >$10^5$°C /sec, atomized powder with -325 mesh | >370°C <450°C | 400°C 11:1 ratio | <6% | bal. | <1% | bal. | >30% | <3% | <5% | >1000MP | >300°C |
| Examples | Er,Yb | Ni,Co | Sc,Y | Mg | 7%<sum(Er,Yb)<8% sum(Ni,Co)<5.5 % sum(Sc,Y)<5%, Mg<3% | about $10^6$°C /sec | 425°C | 400°C 11:1 ratio | | 100 % or <20 % | | bal. | >28% <32% | <3% | <15-20% | 490VHN (1A) which is > 1000MPa | |
| | | | | | | Preferred Methods: | | | | | | | | | | | |
| | | | | | | Atomization and consolidation | | | | | | | | | | | |
| | | | | | | with extrusion | | | | | | | | | | | |

Variations of the described aluminum alloy as well as the process for manufacture thereof and the product created by the process are available to provide the expected functionality of high short-term and long-term strength at temperatures above about 300°C. Thus the invention is to be limited only by the following claims and equivalents thereof.

## CLAIMS

What is claimed is:

1. An aluminum alloy characterized by high strength including high strength in the temperature range greater than about 250°C comprising, in combination:

an alloy mixture in primarily crystalline form having at least about 30% by volume fcc phase and at least about 10% by volume $L1_2$ ductile precipitate phase, said alloy consisting essentially of at least one transition metal selected from the group consisting of about 2 to 12 atomic percent Ni, Co, Ti, Fe, Y, Sc, Cu, Zn, V, Cr, Mn and Li, and at least one rare earth material selected from the group consisting of about 2 to 15 atomic percent Er, Tm, Yb, Lu, and the balance Al.

2. The alloy of claim 1 further including Mg in an amount up to about 5% atomic fraction.

3. The alloy of claim 1 having a tensile strength of at least about 275Mpa at 250°C.

4. A method for manufacture of an aluminum alloy characterized by high strength including high strength in a temperature range greater than about 250°C comprising the steps of:

(a) forming a melt mixture of aluminum, about 2 to about 12 atomic percent of at least one metal selected from the group consisting of Ni, Co, Ti, Fe, Y, Sc, Cu, Zn, V, Cr, Mn and Li, and at least one rare earth selected from the group consisting of about 2 to 15 atomic percent Er, Tm, Yb, and Lu;

(b) converting said melt to an amorphous state wherein the mixture comprises at least about 70% by volume amorphous material; and

(c) devitrifying said amorphous material to at least in part a crystalline matrix of at least about 30% by volume fcc and at least about 10% by volume $L1_2$ phase.

5. The method of claim 4 wherein the step of converting the melt comprises cooling in the range of at least about $10^3$°C per second.

6. The method of claim 4 wherein the step of devitrification is selected from a group consisting of thermoprocessing, thermomechanical processing and combinations thereof.A high temperature and high strength aluminum-based alloy processed through a primarily greater than about 70% in volume amorphous state and then devitrified into greater than about 70% in volume crystalline microstructure with fcc matrix and strengthening by about a ductile $L1_2$ precipitate phase greater than about 10% $L1_2$, and fcc greater than about 30% in volume.

7. The method of claim 4 wherein converting the melt comprises a step selected from the group consisting of gas powder atomization, water powder atomization, melt spinning, spray casting and combinations thereof.

8. The method of claim 4 wherein the step of devitrifying amorphous material comprises a step selected from the group consisting of hot isostatic pressing, thermal aging, extrusion and combinations thereof.

9. An aluminum alloy characterized by high strength including high strength at a temperature greater than about 250°C made by a process comprising the steps of:

(a) formulating a melt comprised of Al; at least one transition metal (TM) selected from the group consisting of Ni, Co, Ti, Fe, Y, Sc, Cu, Zn, V, Cr, Mn, Li and Mg; and at least one rare earth selected from the group consisting of Er, Tm, Yb, Lu;

(b) converting the melt to at least about 70% by volume amorphous material; and

(c) devitrifying at least in part the amorphous material to a mixture of fcc and $L1_2$ crystalline precipitate phase material.

10. The alloy product by the process of claim 9 wherein the transition metal is provided in an amount of about 2 to 10 atomic percent.

11. The alloy product by the process of claim 9 wherein the rare earth material is provided in an amount of about 2 to 10 atomic percent.

12. The alloy product by the process of claim 9 further including an additive of Mg to the melt.

13. The alloy product by the process of claim 9 wherein devitrifying the amorphous material comprises forming at least about 30% by volume fcc material.

14. The alloy product by the process of claim 9 wherein devitrifying the amorphous material comprises forming at least 10% by volume $L1_2$ material.

15. The alloy product by the process of claim 9 wherein converting the melt to amorphous material comprises at least one step selected from the group consisting of gas powder atomization, water powder atomization and melt spinning.

16. The alloy product by the process of claim 9 wherein devitrification comprises at least one step selected from the group consisting of hot isostatic pressing, thermal aging, and extrusion.

17. The method of claim 4 wherein converting the melt comprises the step of rapid solidification processing.

18. The product by the process of claim 9 wherein converting the melt comprises rapid solidification processing.

19. The alloy of claim 1 or claim 9 wherein the precipitate phase has a grain size diameter in the range of less than about 80 nm.

5

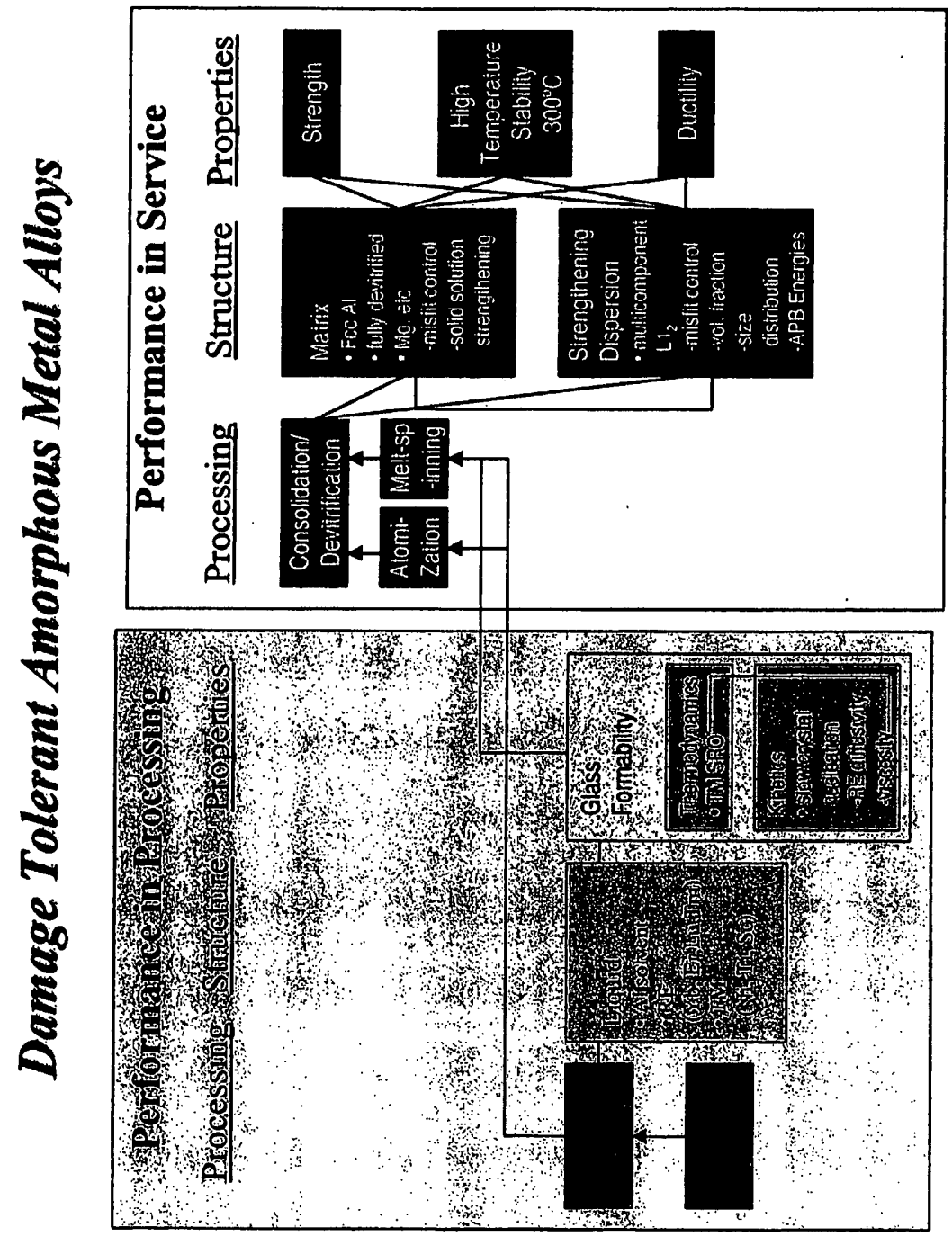
Damage Tolerant Amorphous Metal Alloys
Performance in Processing
Processing Structure Properties
Performance in Service
Processing Structure Properties
Consolidation/ Devitrification
Atomi-Zation
Melt-sp -inning
Matrix
• Fcc Al
• fully devitrified
• Mg, etc
-misfit control
-solid solution strengthening
Strengthening Dispersion
• multicomponent $L1_2$
-misfit control
-vol. fraction
-size
-distribution
-APB Energies
Strength
High Temperature Stability 300°C
Ductility
Glass Formability
Thermodynamics
Kinetics

Figure 1

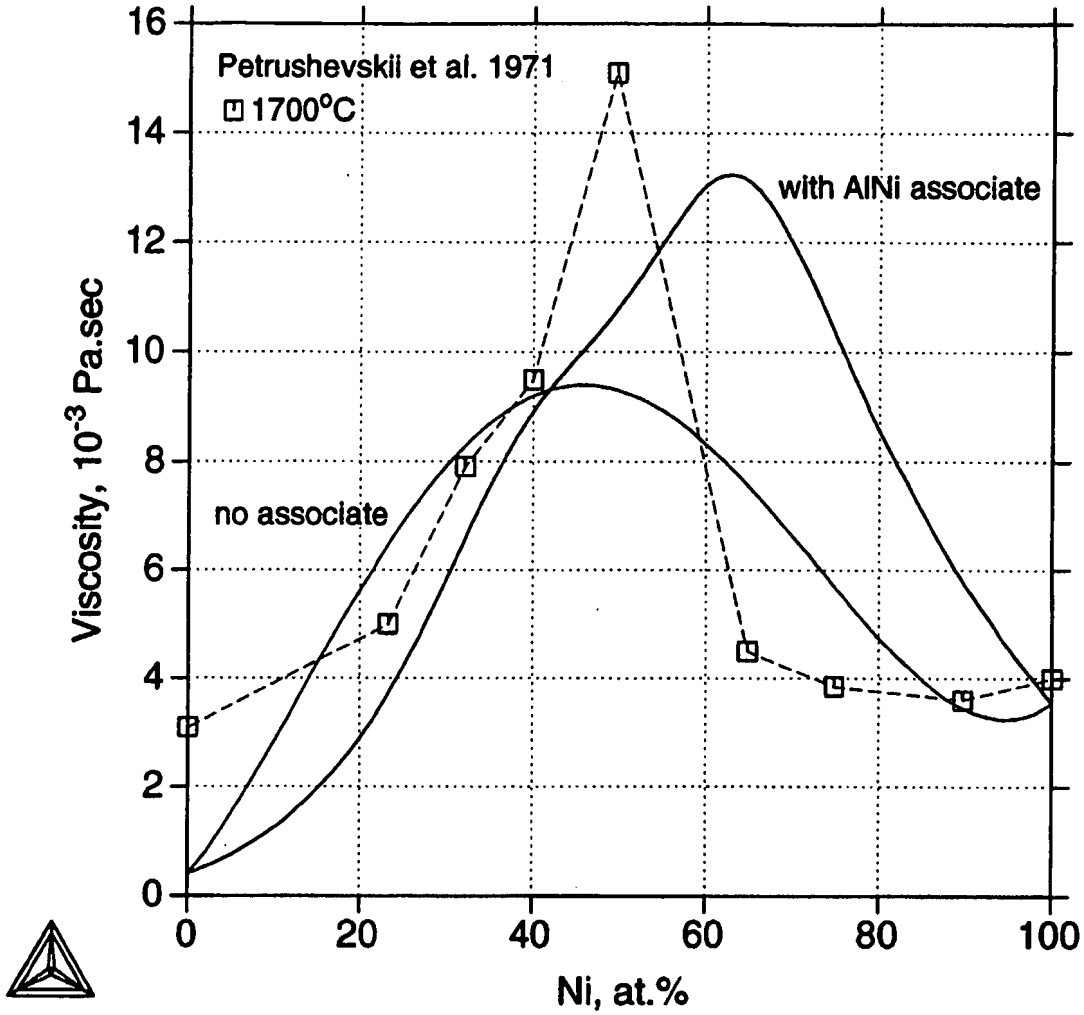
Petrushevskii et al. 1971
1700°C
with AlNi associate
no associate
Viscosity, 10-3 Pa.sec
Ni, at.%
0
2
4
6
8
10
12
14
16
0
20
40
60
80
100

Figure 2

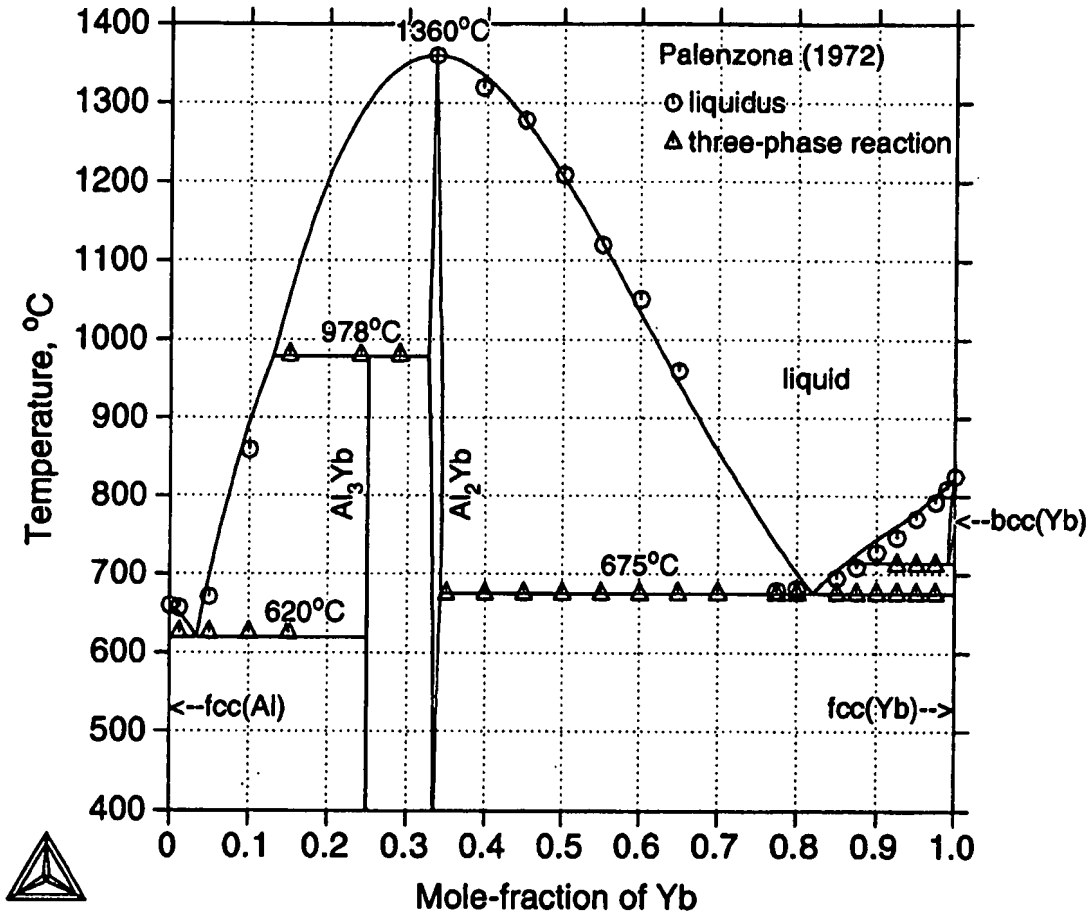
1400
1300
1200
1100
1000
900
800
700
600
500
400
Temperature, °C
0
0.1
0.2
0.3
0.4
0.5
0.6
0.7
0.8
0.9
1.0
Mole-fraction of Yb
1360°C
Palenzona (1972)
liquidus
three-phase reaction
978°C
liquid
Al3Yb
Al2Yb
675°C
620°C
<--bcc(Yb)
<--fcc(Al)
fcc(Yb)-->

Figure 3

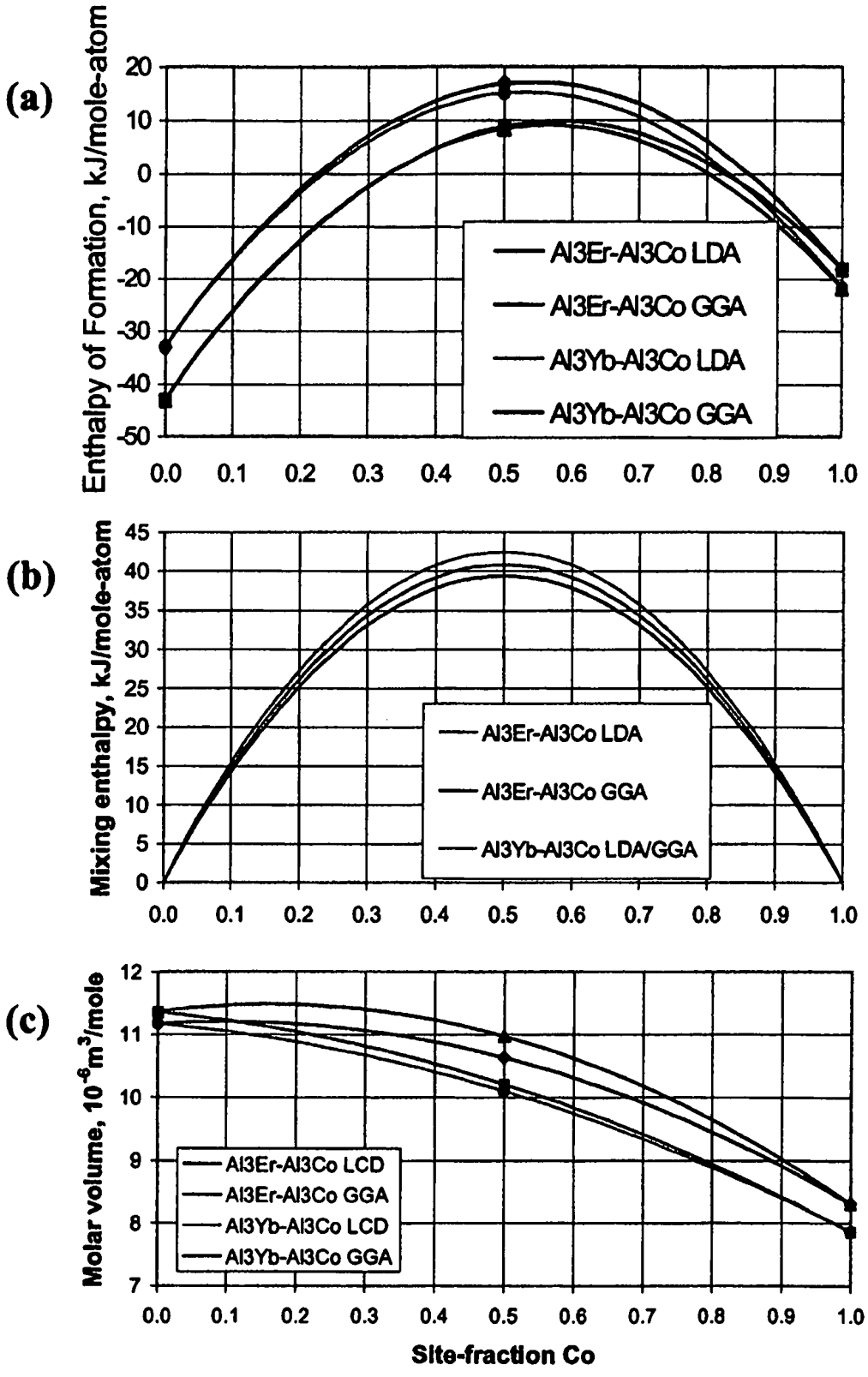
(a)
Enthalpy of Formation, kJ/mole-atom
20
10
0
-10
-20
-30
-40
-50
0.0
0.1
0.2
0.3
0.4
0.5
0.6
0.7
0.8
0.9
1.0
Al3Er-Al3Co LDA
Al3Er-Al3Co GGA
Al3Yb-Al3Co LDA
Al3Yb-Al3Co GGA
(b)
Mixing enthalpy, kJ/mole-atom
45
40
35
30
25
20
15
10
5
0
Al3Er-Al3Co LDA
Al3Er-Al3Co GGA
Al3Yb-Al3Co LDA/GGA
(c)
Molar volume, 10-6m3/mole
12
11
10
9
8
7
Al3Er-Al3Co LCD
Al3Er-Al3Co GGA
Al3Yb-Al3Co LCD
Al3Yb-Al3Co GGA
Site-fraction Co

Figure 4

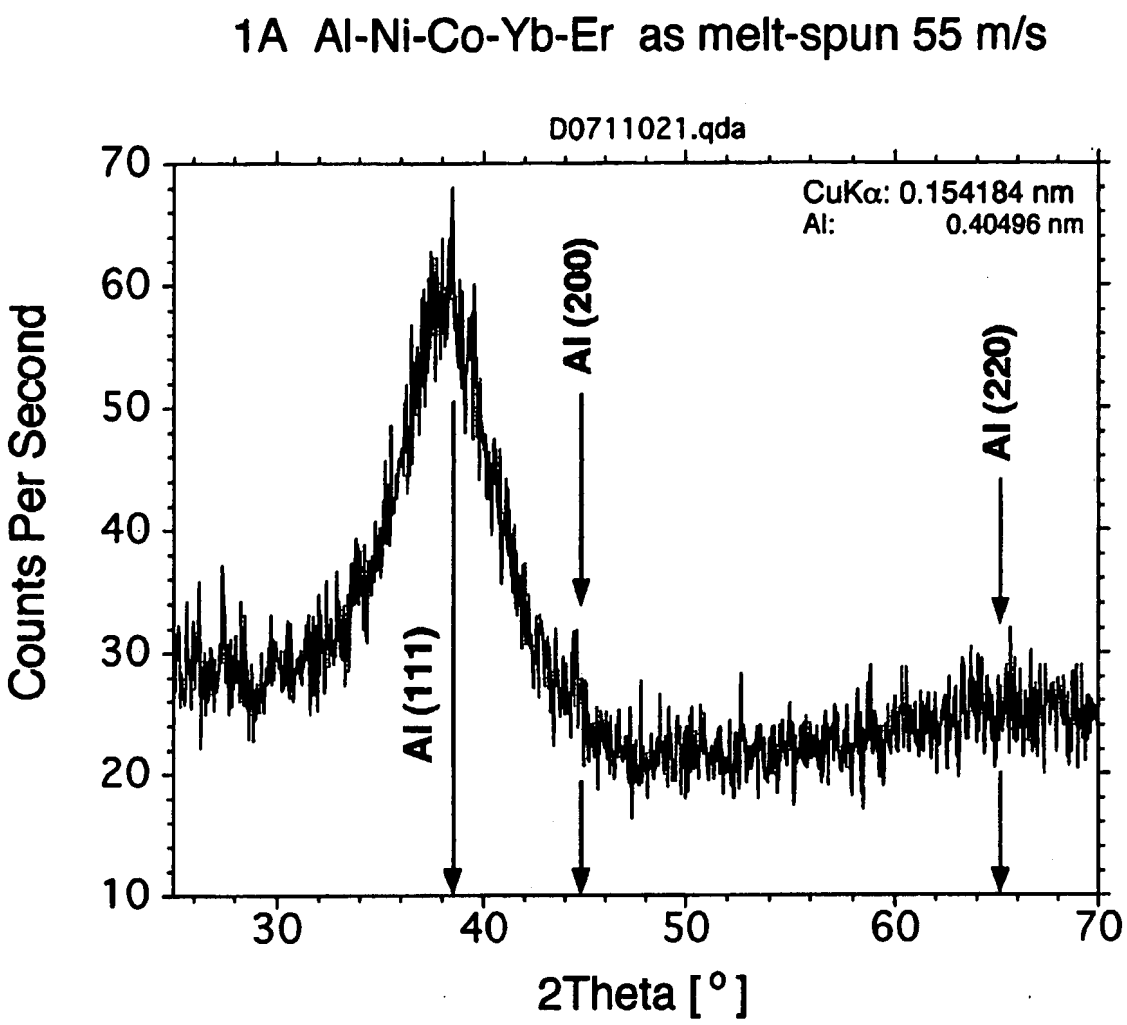
1A Al-Ni-Co-Yb-Er as melt-spun 55 m/s
D0711021.qda
CuKα: 0.154184 nm
Al: 0.40496 nm
Al (111)
Al (200)
Al (220)
Counts Per Second
2Theta [°]
10
20
30
40
50
60
70
30
40
50
60
70

Figure 5

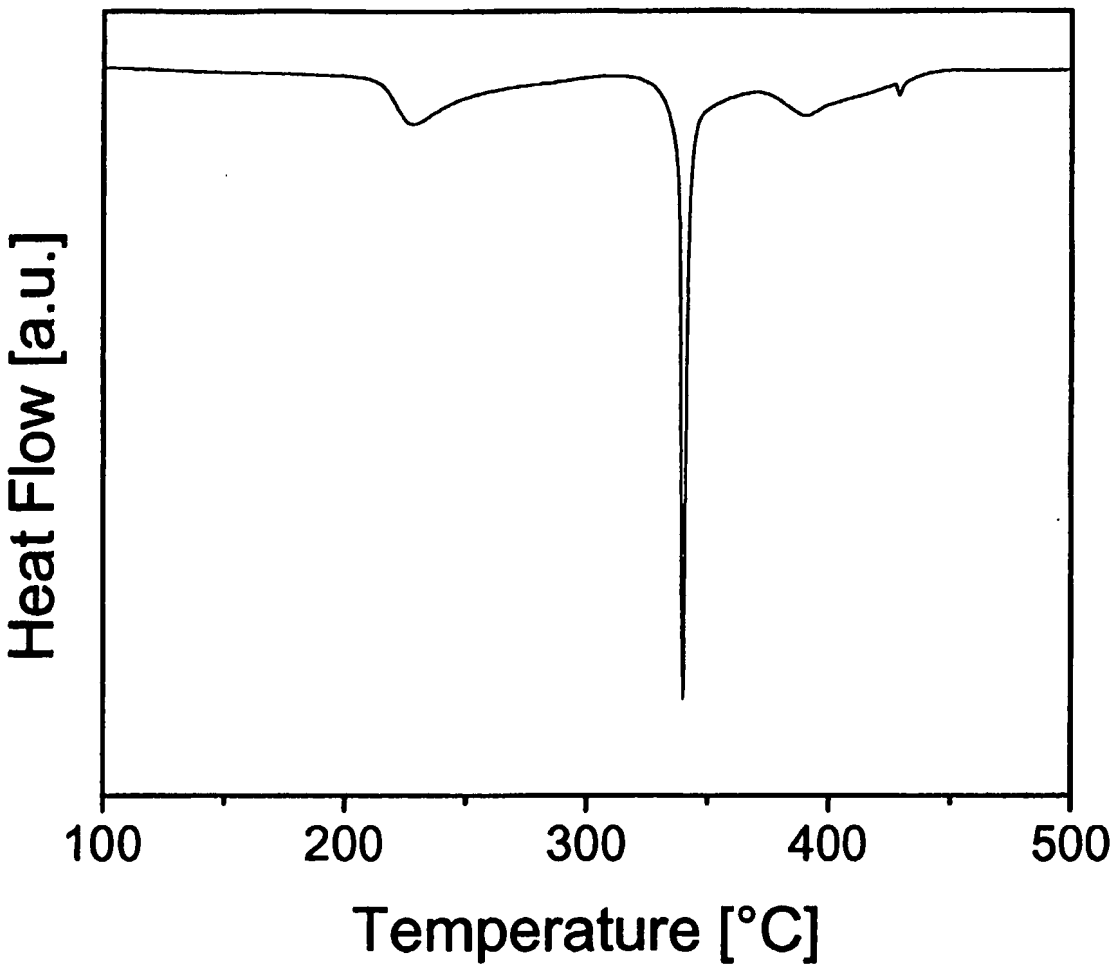


Figure 6

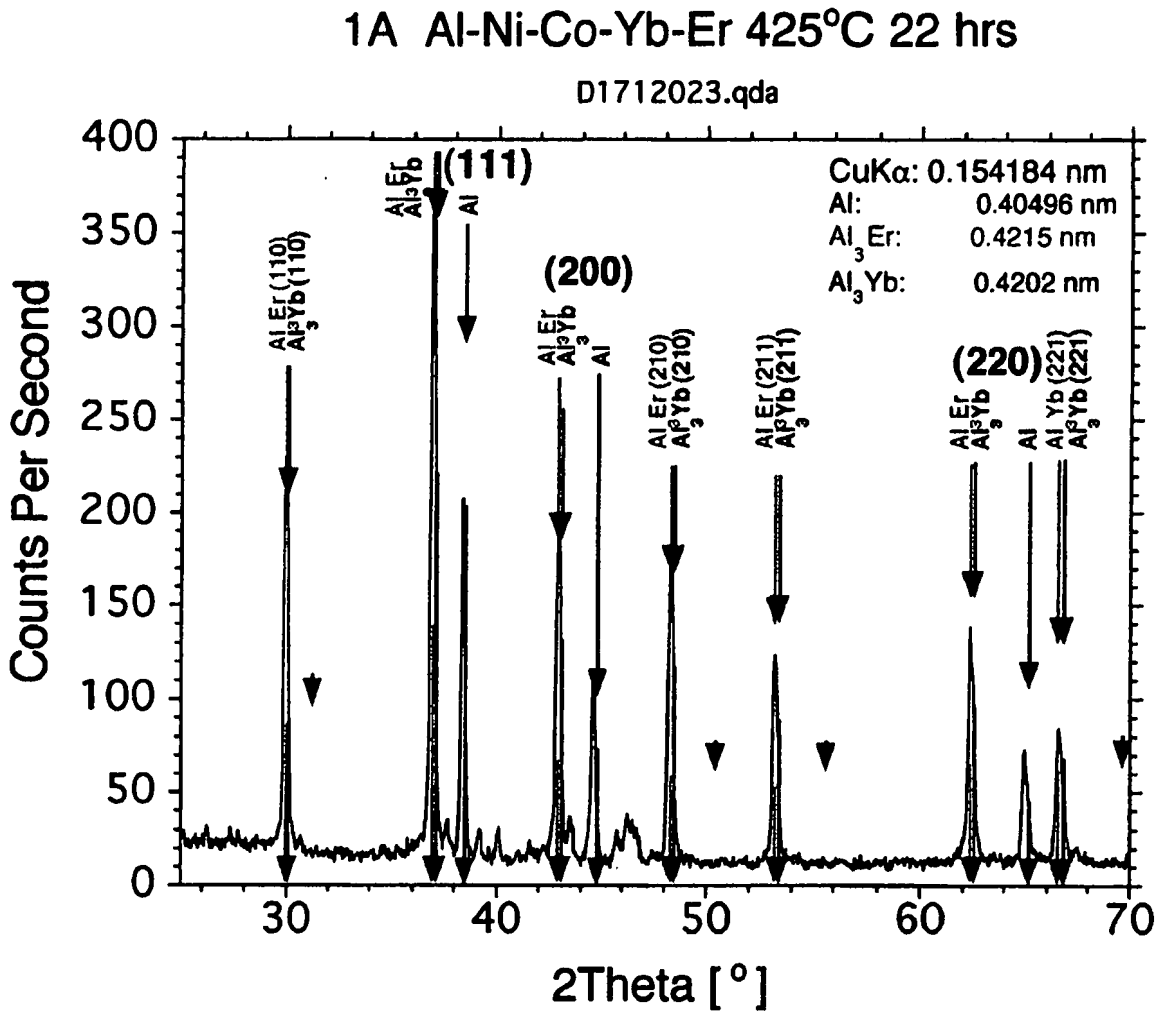
1A Al-Ni-Co-Yb-Er 425°C 22 hrs
D1712023.qda
CuKα: 0.154184 nm
Al: 0.40496 nm
Al3Er: 0.4215 nm
Al3Yb: 0.4202 nm
(111)
(200)
(220)
Counts Per Second
2Theta [°]
0
50
100
150
200
250
300
350
400
30
40
50
60
70

Figure 7

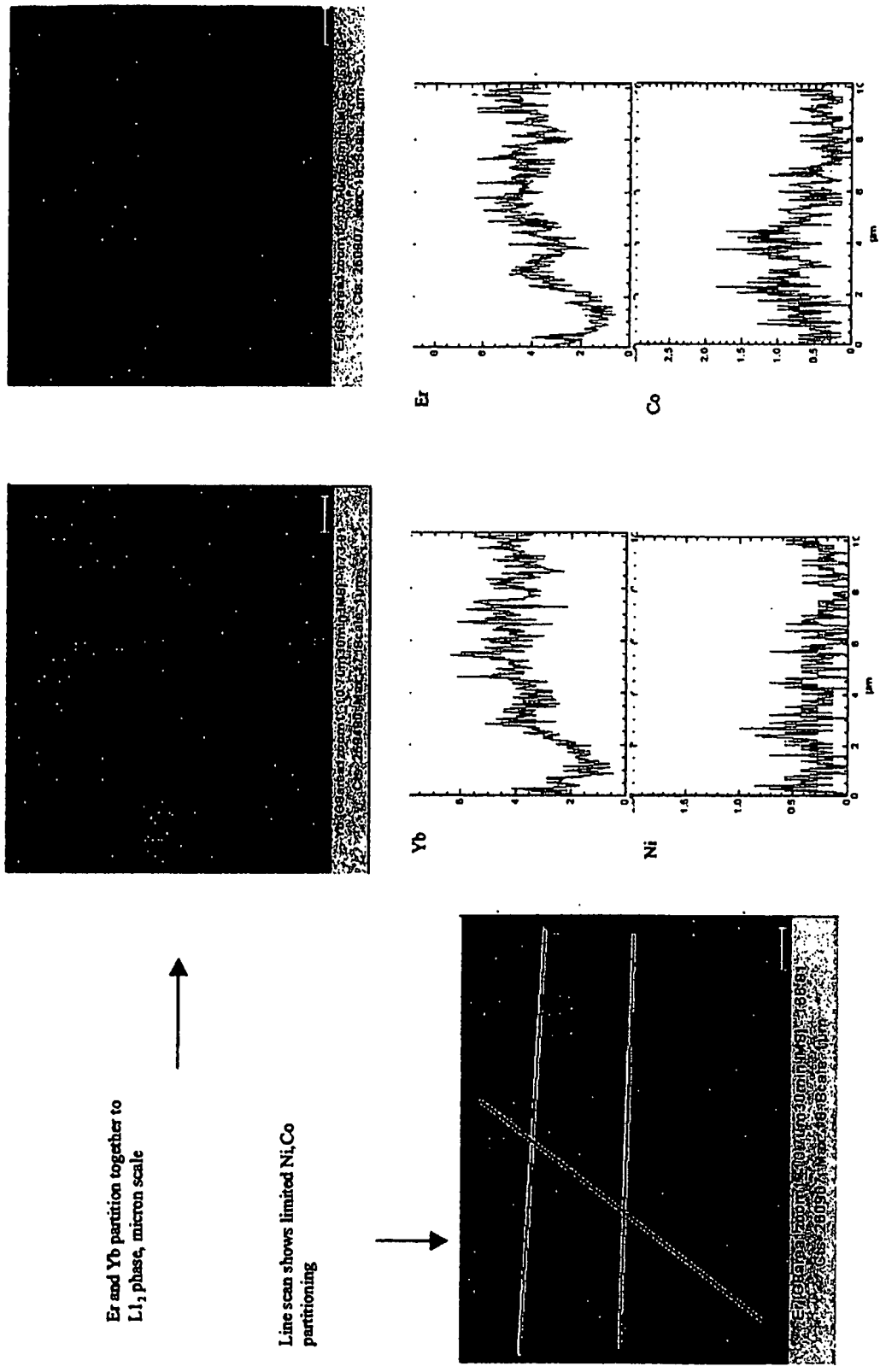
Er and Yb partition together to L1$_2$ phase, micron scale
Line scan shows limited Ni,Co partitioning
Er
Yb
Ni
Co
μm

Figure 8

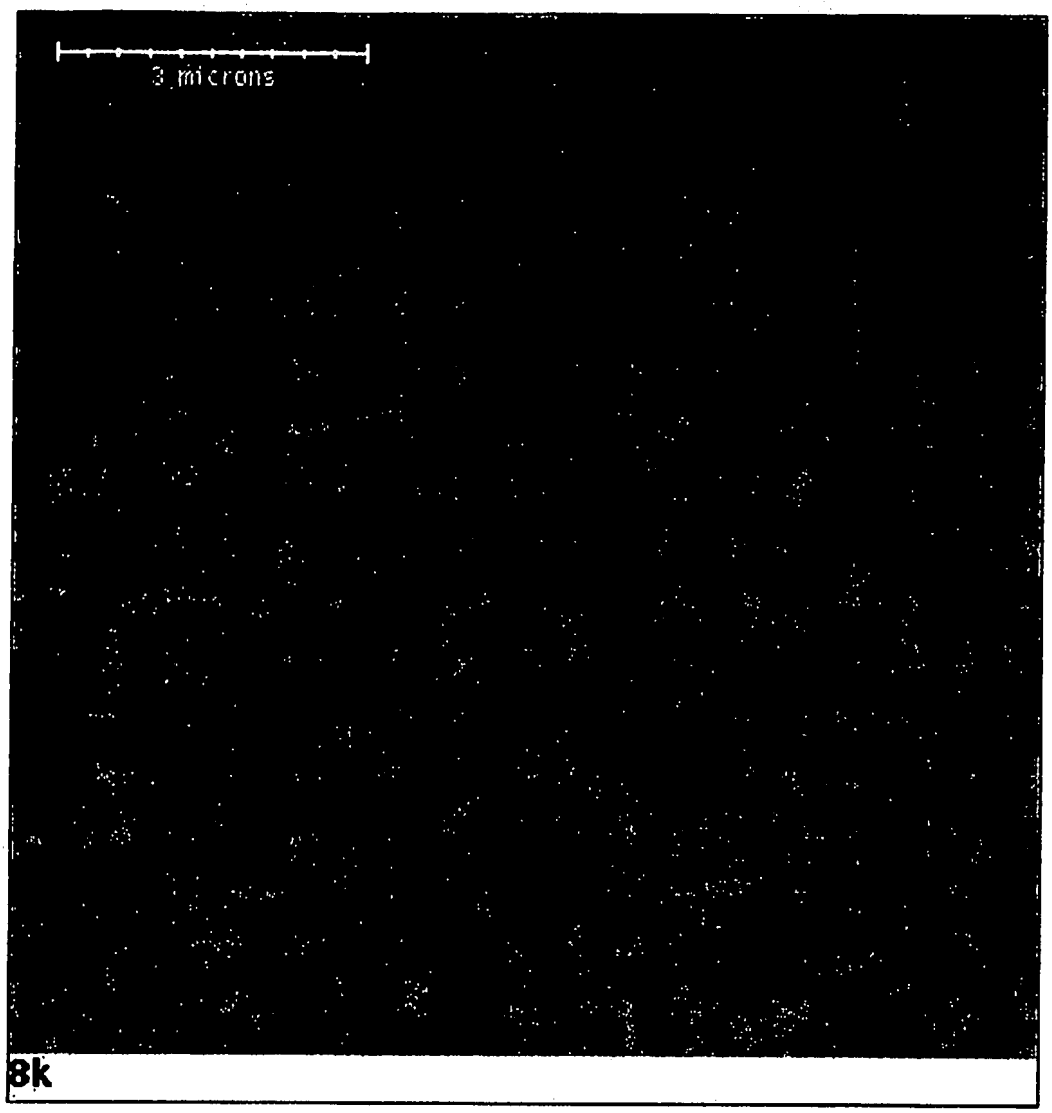


Figure 9

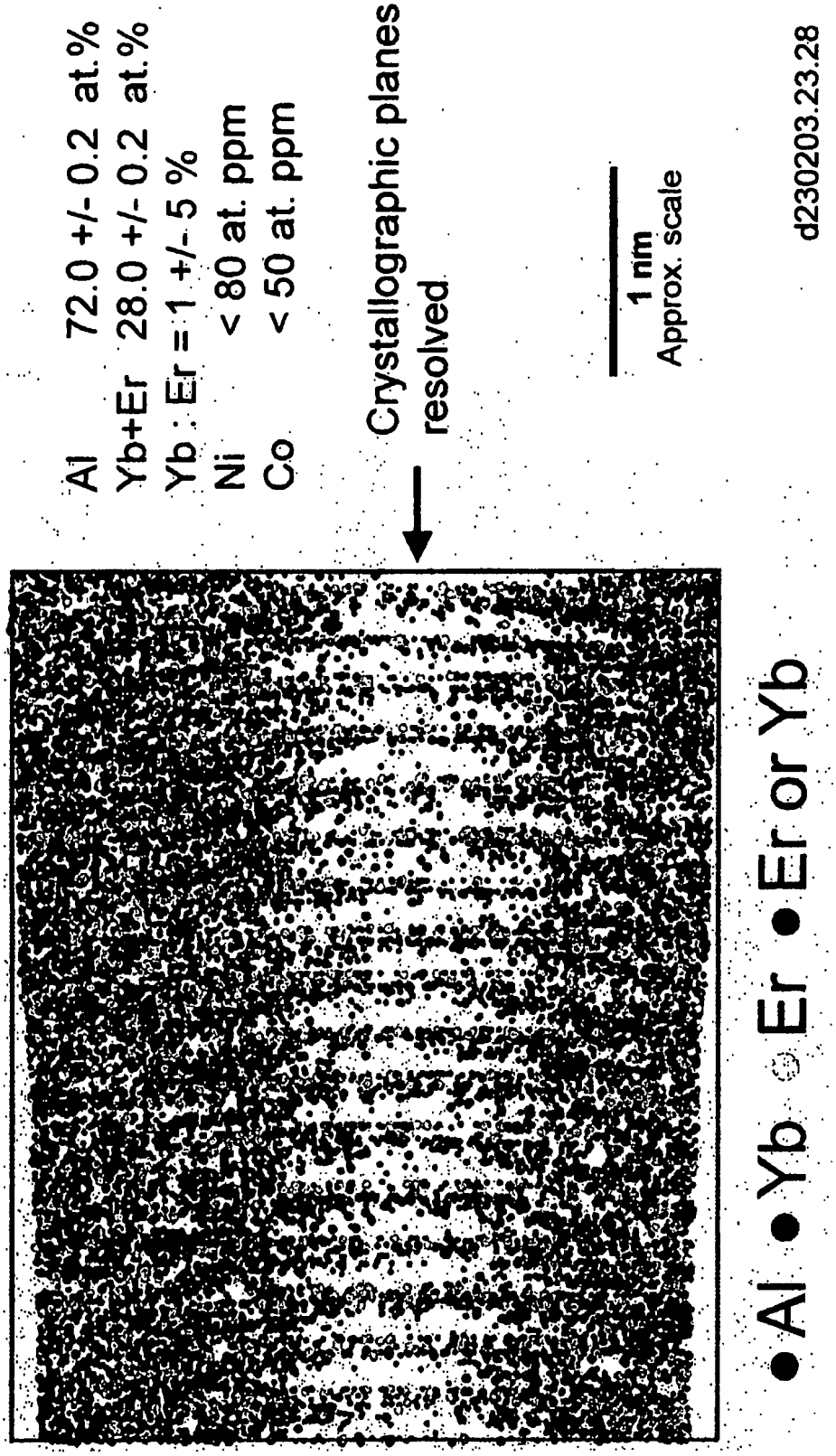
Al 72.0 +/- 0.2 at.%
Yb+Er 28.0 +/- 0.2 at.%
Yb : Er = 1 +/- 5 %
Ni < 80 at. ppm
Co < 50 at. ppm
Crystallographic planes resolved
1 nm
Approx. scale
d230203.23.28
● Al ● Yb ○ Er ● Er or Yb

Figure 10

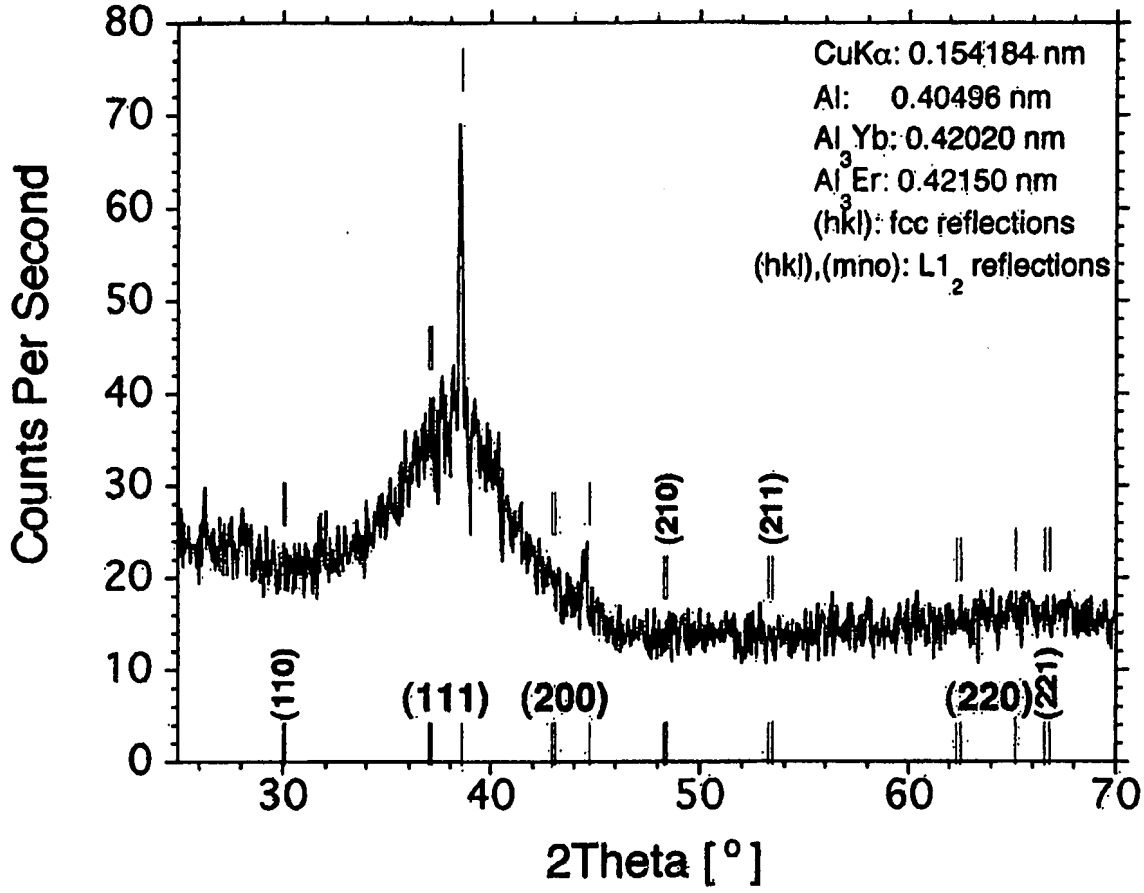
CuKα: 0.154184 nm
Al: 0.40496 nm
Al3Yb: 0.42020 nm
Al3Er: 0.42150 nm
(hkl): fcc reflections
(hkl),(mno): L12 reflections
Counts Per Second
2Theta [°]
(110)
(111)
(200)
(210)
(211)
(220)
(221)

Figure 11

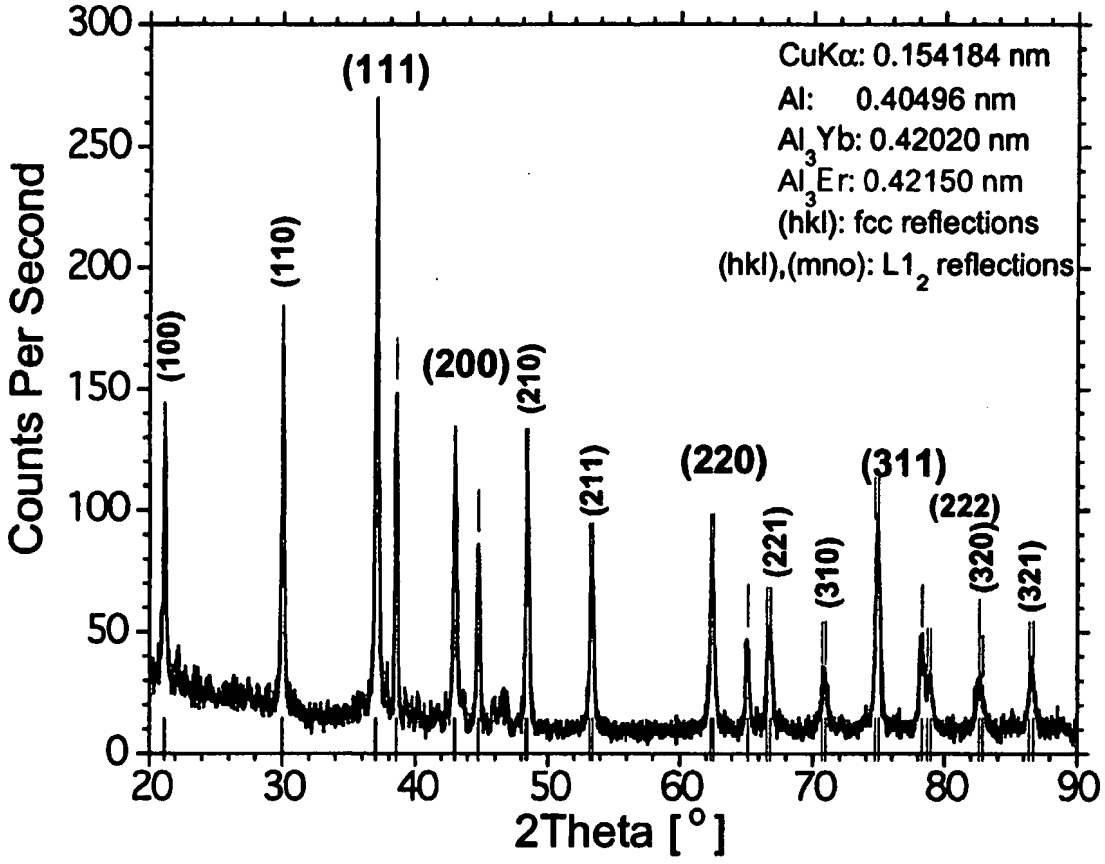
CuKα: 0.154184 nm
Al: 0.40496 nm
Al3Yb: 0.42020 nm
Al3Er: 0.42150 nm
(hkl): fcc reflections
(hkl),(mno): L12 reflections
Counts Per Second
2Theta [°]
(100)
(110)
(111)
(200)
(210)
(211)
(220)
(221)
(310)
(311)
(222)
(320)
(321)

Figure 12

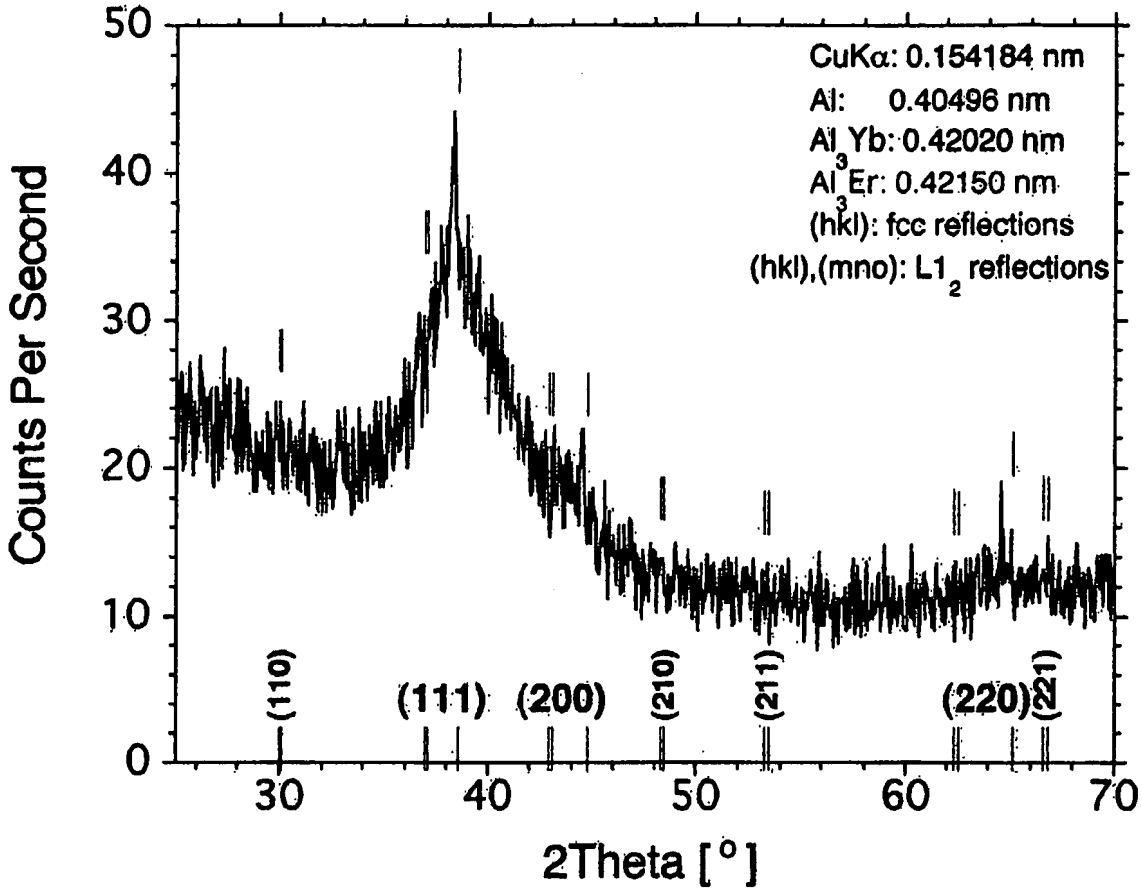
CuKα: 0.154184 nm
Al: 0.40496 nm
Al3Yb: 0.42020 nm
Al3Er: 0.42150 nm
(hkl): fcc reflections
(hkl),(mno): L12 reflections
Counts Per Second
2Theta [°]
(110)
(111)
(200)
(210)
(211)
(220)
(221)
0
10
20
30
40
50
30
40
50
60
70

Figure 13

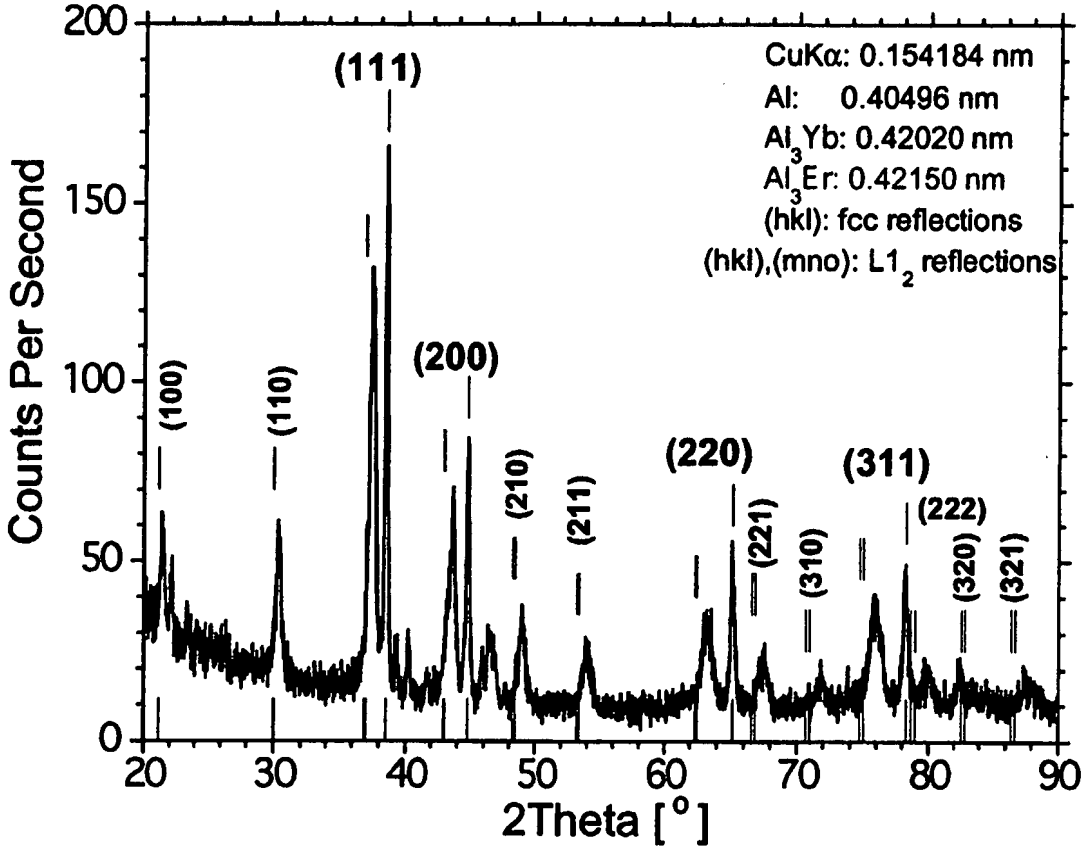
CuKα: 0.154184 nm
Al: 0.40496 nm
Al3Yb: 0.42020 nm
Al3Er: 0.42150 nm
(hkl): fcc reflections
(hkl),(mno): L12 reflections
(100)
(110)
(111)
(200)
(210)
(211)
(220)
(221)
(310)
(311)
(222)
(320)
(321)
Counts Per Second
2Theta [°]
0
50
100
150
200
20
30
40
50
60
70
80
90

Figure 14

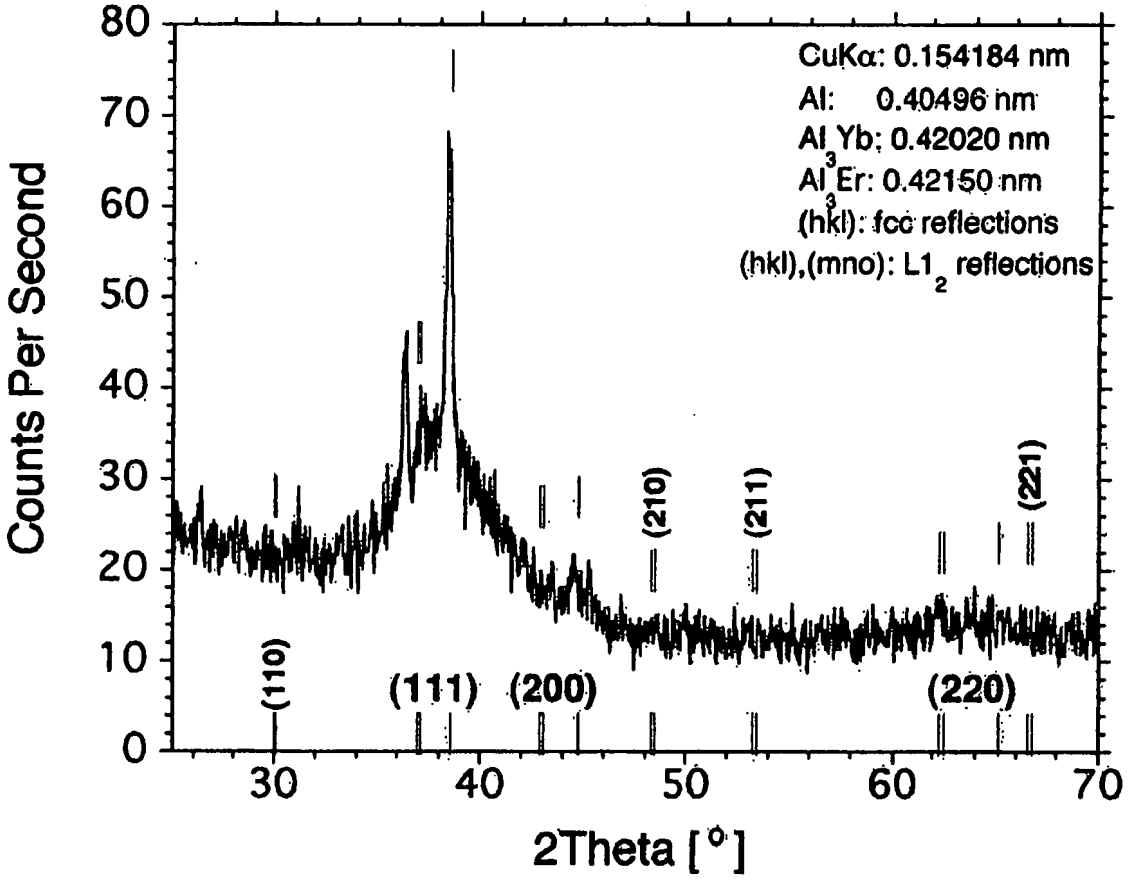
CuKα: 0.154184 nm
Al: 0.40496 nm
Al3Yb: 0.42020 nm
Al3Er: 0.42150 nm
(hkl): fcc reflections
(hkl),(mno): L12 reflections
Counts Per Second
2Theta [°]
(110)
(111)
(200)
(210)
(211)
(220)
(221)
0
10
20
30
40
50
60
70
80
30
40
50
60
70

Figure 15

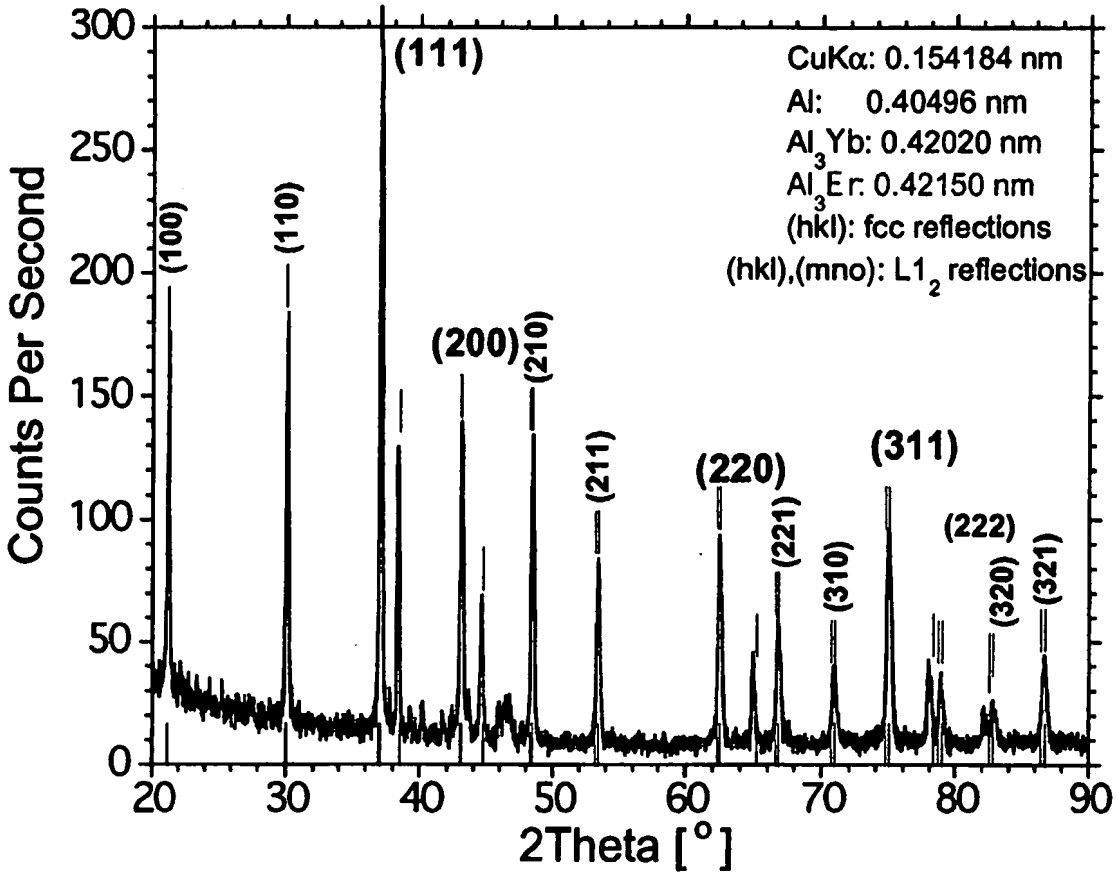
Counts Per Second
2Theta [°]
(111)
(100)
(110)
(200)
(210)
(211)
(220)
(221)
(310)
(311)
(222)
(320)
(321)
CuKα: 0.154184 nm
Al: 0.40496 nm
Al3Yb: 0.42020 nm
Al3Er: 0.42150 nm
(hkl): fcc reflections
(hkl),(mno): L12 reflections

Figure 16

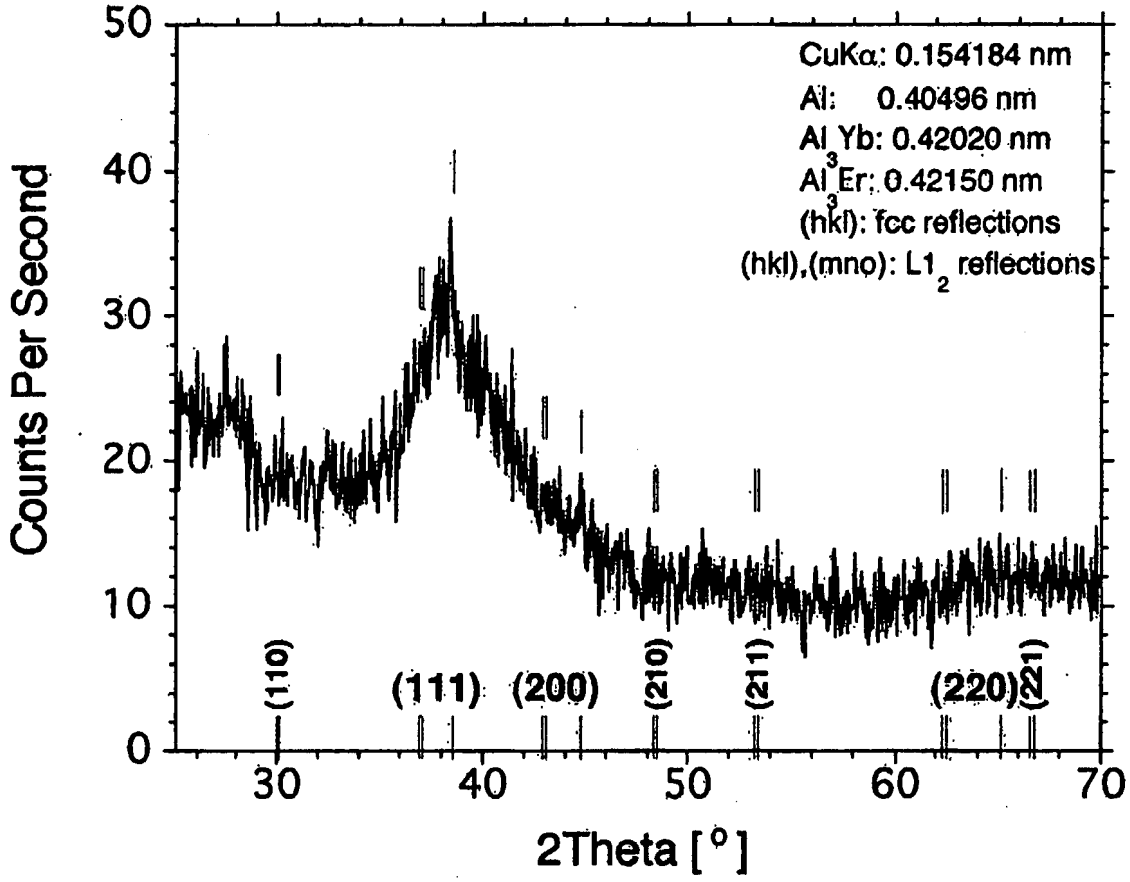
CuKα: 0.154184 nm
Al: 0.40496 nm
Al3Yb: 0.42020 nm
Al3Er: 0.42150 nm
(hkl): fcc reflections
(hkl),(mno): L12 reflections
Counts Per Second
2Theta [°]
(110)
(111)
(200)
(210)
(211)
(220)
(221)

Figure 17

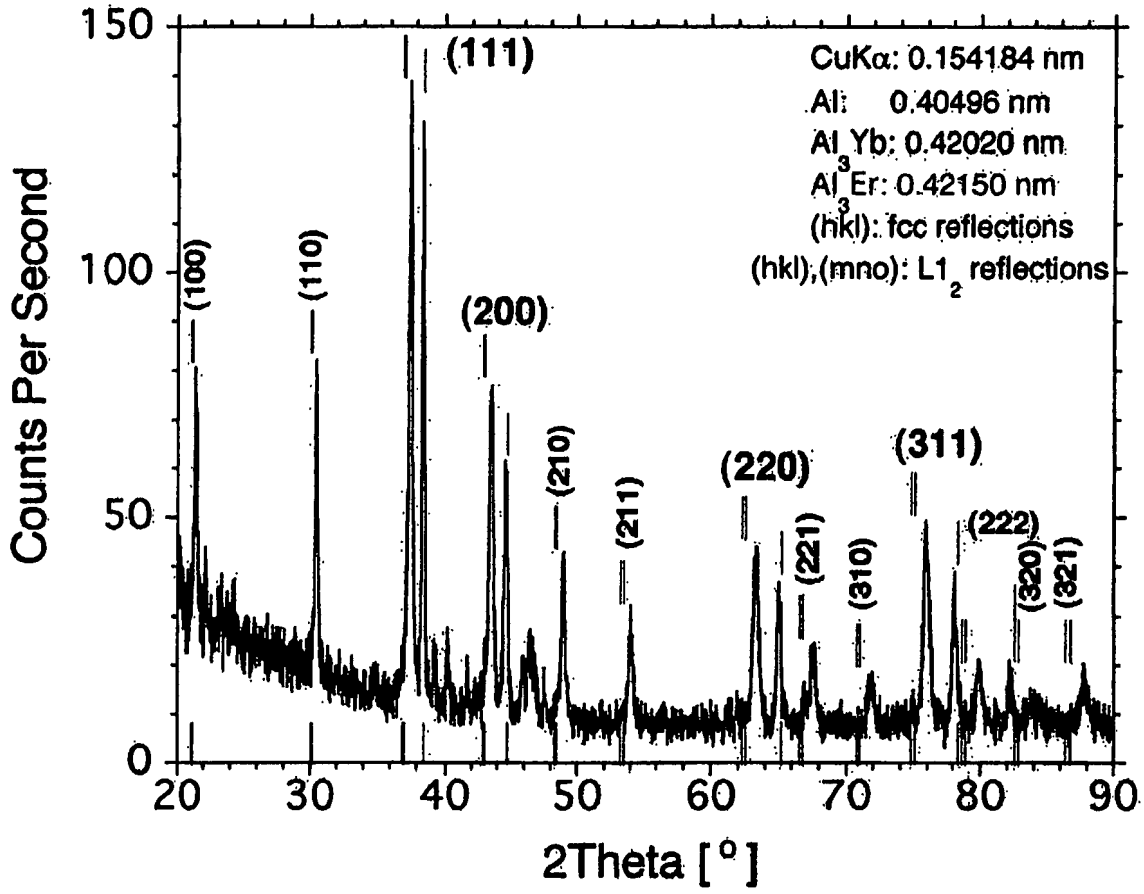
150
100
50
0
Counts Per Second
20
30
40
50
60
70
80
90
2Theta [°]
(100)
(110)
(111)
(200)
(210)
(211)
(220)
(221)
(310)
(311)
(222)
(320)
(321)
CuKα: 0.154184 nm
Al: 0.40496 nm
Al3Yb: 0.42020 nm
Al3Er: 0.42150 nm
(hkl): fcc reflections
(hkl),(mno): L12 reflections

Figure 18

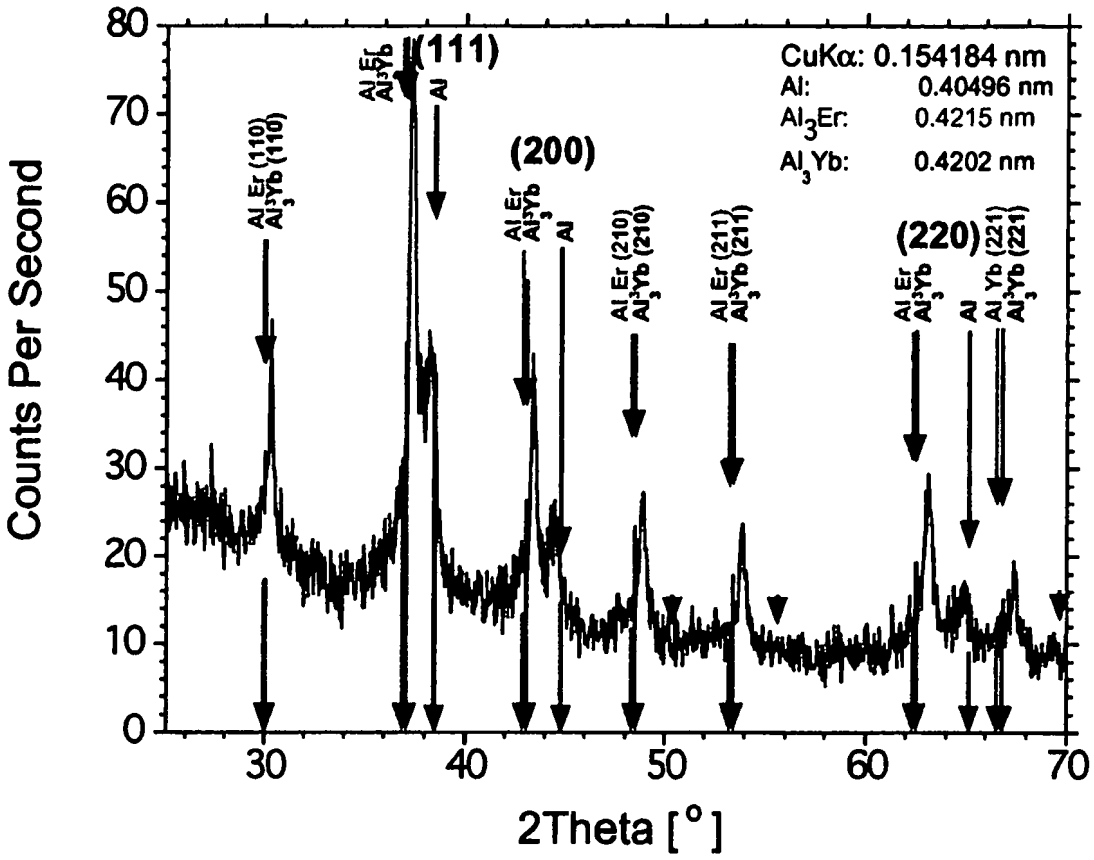
Counts Per Second
2Theta [°]
CuKα: 0.154184 nm
Al: 0.40496 nm
Al3Er: 0.4215 nm
Al3Yb: 0.4202 nm
(111)
(200)
(220)
Al Er Al3Yb (110)
Al Er Al3Yb
Al
Al Er Al3Yb
Al
Al Er (210) Al3Yb (210)
Al Er (211) Al3Yb (211)
Al Er Al3Yb
Al
Al Yb (221) Al3Yb (221)

Figure 19

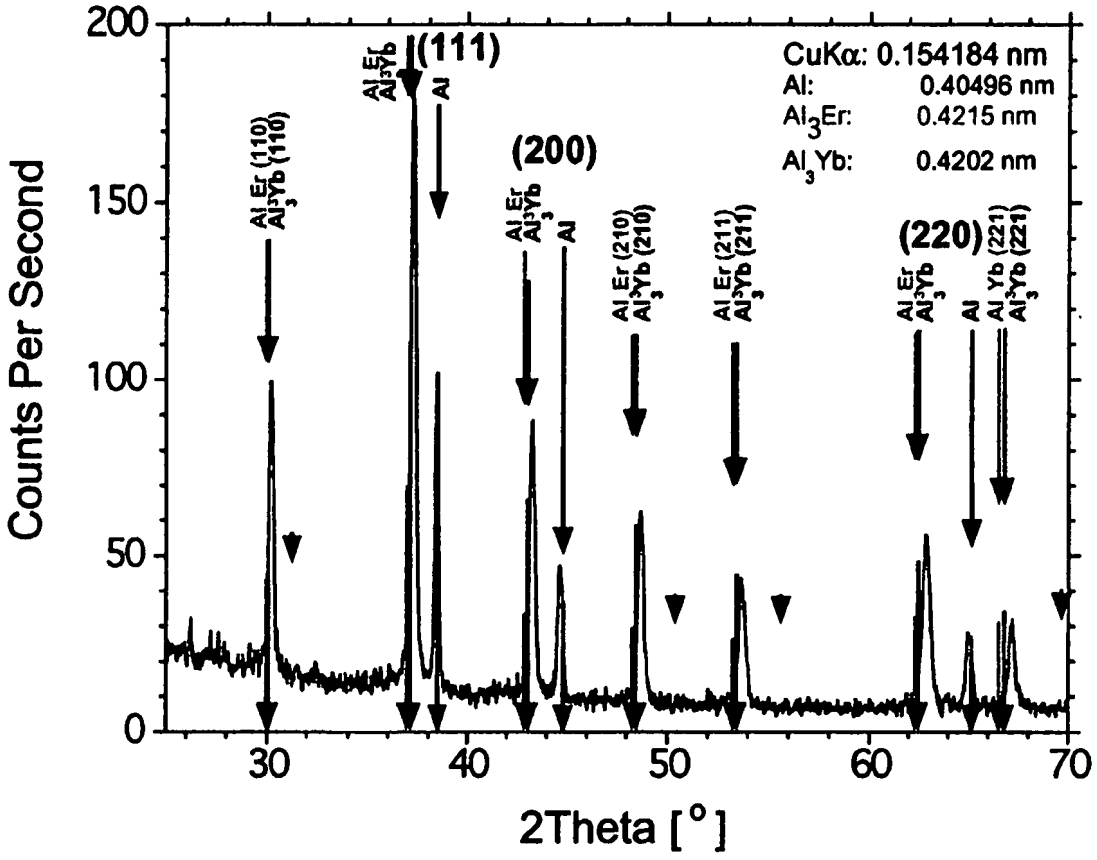
Counts Per Second
2Theta [°]
CuKα: 0.154184 nm
Al: 0.40496 nm
Al3Er: 0.4215 nm
Al3Yb: 0.4202 nm
(111)
(200)
(220)
Al Er Al3Yb
Al
Al Er (110) Al3Yb (110)
Al Er Al3Yb
Al
Al Er (210) Al3Yb (210)
Al Er (211) Al3Yb (211)
Al Er Al3Yb
Al
Al Yb (221) Al3Yb (221)

Figure 20

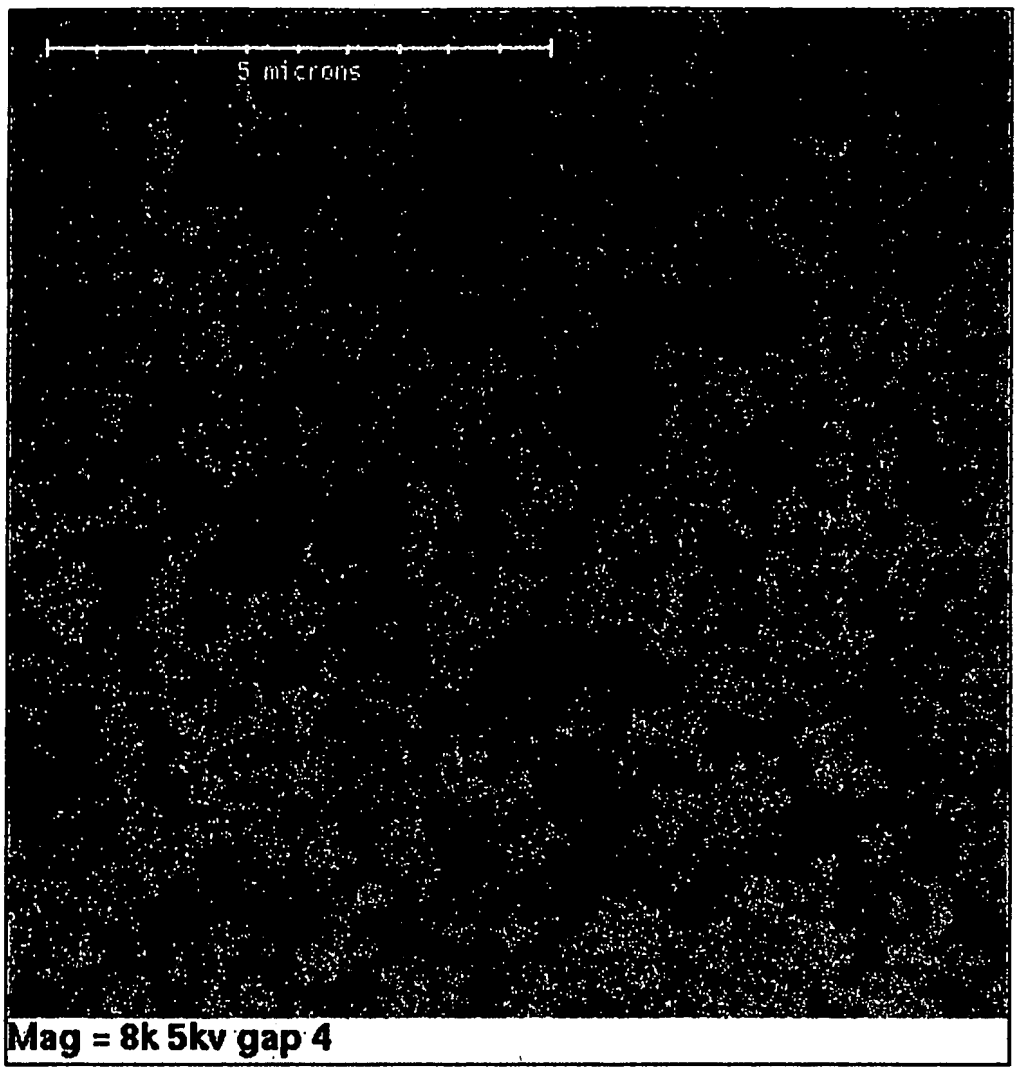


Figure 21